Journal of Power Sources 234 (2013) 310–332

Contents lists available at SciVerse ScienceDirect

Journal of Power Sources

journal homepage: www.elsevier.com/locate/jpowsour

Review

Nanostructured thin film electrodes for lithium storage and all-solid-state thin-film lithium batteries

Yong-Ning Zhou [a], Ming-Zhe Xue [b], Zheng-Wen Fu [a,*]

[a] Department of Chemistry & Laser Chemistry Institute, Shanghai Key Laboratory of Molecular Catalysts and Innovative Materials, Fudan University, Shanghai 200433, PR China
[b] School of Automotive Studies, Clean Energy Automotive Engineering Center, Tongji University, Shanghai 201804, PR China

HIGHLIGHTS

- We reviewed nanostructured thin film electrode for lithium storage and film lithium batteries.
- We summarized thin film electrodes with various electrochemical reaction mechanisms.
- We described thin film electrodes used in all-solid-state thin film batteries.

ARTICLE INFO

Article history:
Received 26 July 2012
Received in revised form
12 November 2012
Accepted 13 January 2013
Available online 1 March 2013

Keywords:
Lithium storage
Thin film electrodes
All-solid-state thin-film lithium battery
Review

ABSTRACT

Extensive research is underway to yield greater insights into the intrinsic properties of electrode materials for lithium storage. Presently, nanostructured thin-film electrodes without any additives and binders used in powder-based electrodes have been employed as the "ideal" system for fundamental research because of their low resistance, cleanliness and purity. This review summarizes the research on, and progress in such nanostructured thin-film electrode materials for lithium storage and for all-solid-state thin film batteries. Nanostructured thin film electrodes with various electrochemical reaction mechanisms based on nanometer-size effects, chemical composition and structure are summarized. Thin film electrodes used in all-solid-state thin film batteries are also described.

1. Introduction

Energy shortage and environment pollution are among the most important problems facing the world today. There is an urgent need to develop clean energy sources and new energy-storage systems. Lithium-ion batteries (LIBs) have the merits of light weight, high energy density, high power, smooth discharge, and being environment friendly; they are deemed the best choice for portable energy-storage systems. Nowadays, LIBs are widely used in electronic applications and hold much promise as green-power sources for electric vehicles. The electrode's material is one of the key components for perfecting lithium-ion batteries. It plays a crucial role in establishing the overall properties of the battery and presently is the main obstacle in fabricating the next generation of these batteries. Thus, the major objectives of researchers in this field are identifying new electrode materials and improving traditional electrode materials. Over the past few years, with rapid progress in nanotechnology, the usage of nanostructured materials, with their unique properties, has become prominent in many fields. There are special advantages of using nanostructured materials as electrodes. For example, the thickness of a typical nanostructured thin-film electrode usually is less than 200 nm with a particle size smaller than 50 nm (Fig. 1a) [1]. Such kinds of electrodes could significantly reduce the transportation and diffusion length of ions and electrons (Fig. 1b), thereby remarkably enhancing the kinetics of lithium storage.

An all-solid-state thin-film lithium battery (TFB) is a thin battery consisting of a positive and negative thin-film electrode and a solid-state electrolyte. The thickness of a typical one usually is less than 20 μm. It can be used in smart cards, sensors, and also in micro-electromechanical systems (MEMSs). Thin-film electrode material could be obtained by transforming the common electrode materials into a thin-film structure. Since the electronic resistance of the resulting film electrode-material is reduced remarkably, conductive additives, such as carbon black, need not be added. Furthermore, due to the thin film's dense structure, a polymeric binder also is not needed. Therefore, such an electrode is a "pure" system and is

* Corresponding author. Tel.: +86 21 65642522; fax: +86 21 65102777.
E-mail address: zwfu@fudan.edu.cn (Z.-W. Fu).

0378-7753/$ – see front matter © 2013 Elsevier B.V. All rights reserved.
http://dx.doi.org/10.1016/j.jpowsour.2013.01.183

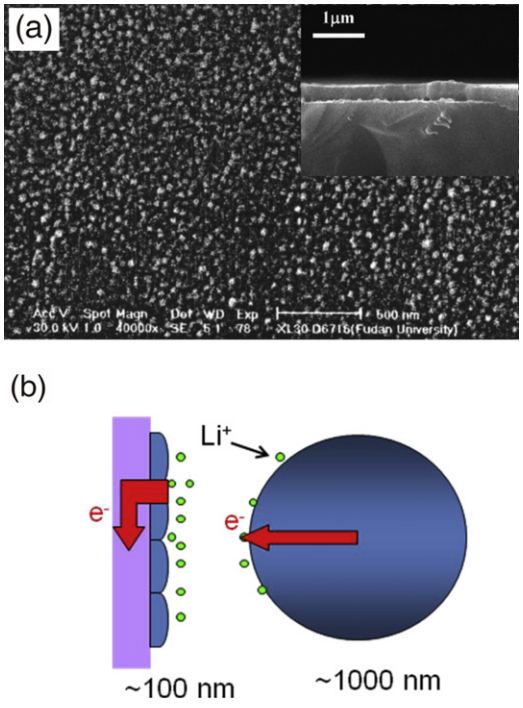

Fig. 1. (a) Surface and cross-sectional morphology of nanosized ZnO thin film; (b) comparison of Li^+ and electron transportation in thin film electrodes and bulk electrodes. Reproduced from Ref. [1].

favorable and convenient for exploring the basis of active electrode materials.

This review focuses on progress in research on nanostructured thin film-based electrodes for lithium-ion batteries and all-solid-state thin film lithium batteries. We will detail the many lithium storage mechanisms based on nanometer-size effects, chemical composition, and structure. The unique characters of thin-film electrodes compared to bulk electrodes are clarified.

2. Fabrication and characterization of thin-film electrodes

A variety of versatile deposition technologies are available to prepare thin-film electrodes, including magnetron sputtering [2], pulsed laser deposition (PLD) [3], electron beam evaporation [4], chemical-vapor deposition [5], electrostatic-spray deposition (ESD) [6], and sol–gel fabrication [7]. Among them, the first two are the most popular ones for fabricating high-quality thin film electrodes. The magnetron sputtering method yields large-scale, uniform, dense thin films with good adhesion between the film and substrate. With pulsed-laser deposition, we can prepare high-quality thin film with same stoichiometric ratio as the target, and is easy to deposit high-melting-point materials. Many approaches are suitable for characterizing the physical and chemical properties of thin-film electrodes, including X-ray diffraction (XRD), X-ray photoelectron spectroscopy (XPS), scanning electron microscopy (SEM), transmission electron microscopy (TEM), selected-area electron diffraction (SAED), Raman spectroscopy, Auger electron spectroscopy (AES), Fourier transform infrared spectroscopy (FTIR), and Mössbauer spectroscopy.

3. Thin-film electrode based on intercalation reaction

3.1. LiMO-type thin-film electrodes

LiMO-type materials (in which M represents various metals), mainly containing layered structures and spinel structures, are the most widely used electrode materials for lithium ion batteries. Layered $LiCoO_2$ was the first commercialized cathode material. Tarascon et al. [8] were the first to propose, via a US patent, the usage of $LiCoO_2$ thin film as the cathode for thin-film lithium-ion batteries. However, they did not show any evidence on such

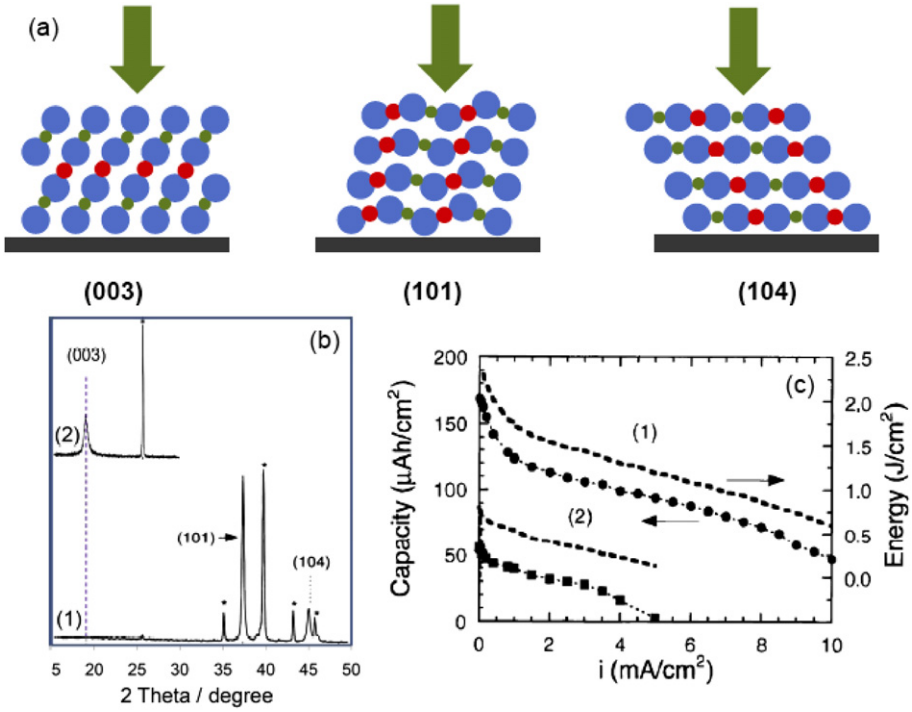

Fig. 2. (a) Illustration of the preferred orientation of the $LiCoO_2$ grains for lithium-ion penetration. (b) XRD patterns of $LiCoO_2$ films with (003) preferred orientation (1), and (101) preferred orientation (2); (c) electrochemical performance of $LiCoO_2$ films with (003) preferred orientation (1), and (101) preferred orientation (2). Reproduced from Ref. [11].

application. Dahn et al. [9] were the first to fabricate $LiCoO_2$ thin films by pulse-laser ablation, noting the existence of both high- and low-temperature $LiCoO_2$ phases after annealing. For such films, the preferred orientation and its relation with substrate significantly affect lithium penetration [10,11]. As shown in Fig. 2a, grains with their (003) planes parallel to the substrate block the flow of lithium, whereas grains with their (101) or (104) planes parallel to the substrate facilitate its flow. The performance of the latter films is much better than that of the former group (Fig. 2b and c). The four key factors determining the preferred orientation of the films are substrate temperature, annealing temperature, film's thickness and deposition methods. Increasing the substrate temperature from room temperature to 500 °C changes the film's structure from an amorphous one to a crystalline one with a strong (003) texture [12]. For the annealing temperature, it was confirmed that annealing $LiCoO_2$ thin film at about 700 °C favors the presence of (101) and (104) planes [13–17]. Regarding thickness, $LiCoO_2$ films over 1 μm tend to have the preferred orientation of (101) and (104) due their propensity for minimizing volume-strain energy, while in films thinner than 0.5 μm, the orientation of (003) predominates as a result of the proneness to minimize surface energy [5]. Exploring the different methods of film deposition, Bouwman et al. [18–20] stated that films deposited by radio-frequency (RF) sputtering exhibited an *a*-axis orientation while those deposited by PLD showed a *c*-axis orientation. Sauvage et al. [21] characterized the *in-situ* conductivity evolution of $LiCoO_2$ thin films during charge–discharge cycling and found that the conductivity of $LiCoO_2$ increased in the solid-solution region.

Since Ni has similar properties as Co but is much cheaper and causes less pollution, many groups attempted to use it to replace Co. However, there are few reports of successfully fabricating crystalline $LiNiO_2$ thin films because of the difficulty in oxidizing Ni^{2+} to Ni^{3+} and the instability of the $LiNiO_2$ layered structure. Thus, Lai et al. [22] synthesized $LiNiO_2$ thin film on a nickel substrate in a LiOH solution by a hydrothermal method. The reaction temperature played an important role in the formation of $LiNiO_2$ phase. When the temperature was under 140 °C, a pure $LiNiO_2$ film did not form due to inadequate oxidative dissolution of the Ni substrate. In contrast, when the temperature reached 200 °C, a pure, uniform $LiNiO_2$ thin film was obtained. Kim et al. [23] prepared $LiNiO_2$ thin film by magnetron sputtering. A well-crystallized $LiNiO_2$ thin film formed after rapid thermal annealing at 700 °C. To stabilize the structure of $LiNiO_2$, substituting some of the Ni by other metal atoms in $LiNiO_2$ structure proved effective. $LiNiCoO_2$ films grown at 250 °C substrate temperature by RF-sputtering exhibited a poorly crystallized layered structure with R3m symmetry [24]. They exhibited poor electrochemical activity, even though they had a (104) preferred orientation. Raising the annealing temperature greatly enhanced their electrochemical performance due to an improvement in their crystallization. Chiu et al. [25,26] fabricated $LiNiO_2$ and $LiNi_{0.8}Co_{0.2}O_2$ polycrystalline thin-films successfully by *in-situ* heating sputtering (350–450 °C); these films do not need annealing at high temperature, which is a considerable advantage in preparing all-solid-state thin-film batteries. Xia et al. [27] generated $LiNi_{0.5}Mn_{0.5}O_2$ thin films by pulsed laser deposition and exposed them to post-annealing treatment at different temperatures. They found that the formation of the well crystallized $LiNi_{0.5}Mn_{0.5}O_2$ film required using a very high annealing temperature of 850 °C; these films exhibited a (003) preferred orientation in the annealing range of 750–950 °C. However, temperatures over 950 °C were detrimental due to the formation of impurity phases.

Besides the layered structure $LiMO_2$, spinel structured $LiMn_2O_4$ is another important group of cathode material for lithium-ion batteries. Striebel et al. [28] fabricated $LiMn_2O_4$ thin films by pulse-laser sputtering with a reversible capacity of 56 μAh cm^{-2} μm^{-1}. The diffusion coefficient of lithium ions was about 2.5×10^{-11} cm^2 s^{-1}. The resulting $LiMn_2O_4$ thin film/$LiClO_4$/Li cell could be cycled for more than 300 times. A drop in discharge capacity of 54% was observed on increasing current density by an order of magnitude. Ueda et al. [29] made a nanocrystalline $LiMn_2O_4$ thin film by magnetron sputtering and characterized its electrochemical performance; it achieved a reversible capacity of 41 μAh cm^{-2} μm^{-1} at the current density of 40 μA cm^{-2} and could withstand more than 1000 cycles. Chiu et al. [30–34] also prepared $LiMn_2O_4$ thin films by the magnetron-sputtering method and the sol–gel method. They optimized the films' properties by oxygen plasma and surface coating. The treated films had a denser microstructure than untreated ones, with better cycling performance and greater stability at high temperatures. Whitacre et al. [35] succeeded in fabricating $Li_yMn_xNi_{2-x}O_4$ thin films by sputtering a $LiMn_2O_4/LiNiO_2$ mixed target. Cathodes with a composition of $LiMn_{1.4}Ni_{0.6}O_4$ had both the highest specific capacity (52 μAh cm^{-2} μm^{-1} or 115 mAh g^{-1}) as well as the longest high-potential (4.7 V) discharge plateau, while cells with higher Mn content had a longer 4 V discharge plateau, a result that qualitatively agrees with similar studies on conventional bulk-fabricated cathodes of the same material.

3.2. Olivine and poly-anion thin-film electrodes

$LiFePO_4$ is the most well-known olivine structure cathode material [36,37]. Due to its excellent structural stability and high power properties, it is considered as one of the most promising cathode material for future lithium ion batteries. Sauvage et al. [38] fabricated a well-crystallized 300 nm $LiFePO_4$ thin film by PLD. It demonstrated good electrochemical performance in both aqueous and non-aqueous electrolytes. Such thin films annealed at 400 °C or lower were not well crystallized, while those annealed at 700 °C or higher were not single-phase $LiFePO_4$ and contained impurities [39,40]. Those annealed at 600 °C exhibited a larger discharge capacity than that annealed at 500 °C, but the rate performance of the former was inferior to the latter. The point of optimization between high rate-capability and large capacity lays between 500 °C and 600 °C. Eftekhari et al. [41] prepared $LiFePO_4$/Au nano-composite thin films by RF sputtering. After 1000 cycles at 80 °C, fading in capacity was only 10%. Chiu et al. [42] investigated the influence of the conditions of preparation via RF magnetron sputtering. They found that $LiFePO_4$ had the best performance when it was deposited at a bias voltage of −50 V and then annealed at 500 °C; reversible capacity then was 170 mAh g^{-1} ± 7.5%. Seemingly, this is an ideal system in which to measure the intrinsic kinetic property of $LiFePO_4$ in a thin-film state [43]. The diffusion coefficients (D_{Li}) of lithium ion in $LiFePO_4$ thin film was measured by three different techniques (CV, GITT and EIS); the D_{Li} obtained by GITT and EIS showed a minimum value at $x \sim 0.5$ for $Li_{1-x}FePO_4$, differing from that obtained by CV. The results suggested that the kinetic parameters for a two-phase transition reaction electrode material could not be measured accurately by GITT or EIS, unless the material was treated and modified. Matsumura et al. [44] compared the electrochemical performances of preferentially oriented PLD thin film electrodes of $LiNi_{0.8}Co_{0.2}O_2$, $LiFePO_4$, and $LiMn_2O_4$. The $LiFePO_4$ films, showing powder-like crystal growth, and the $Li_{1.1}Mn_{1.9}O_4$ films, having a high degree of cubic (111) orientation displayed favorable charge–discharge curves. In contrast, $LiNi_{0.8}Co_{0.2}O_2$ films with a high degree of hexagonal (003) orientation cannot deliver enough discharge capacity compared to the corresponding composite powder electrode. Furthermore, after comparing with a film fabricated by sputtering method, rate performance of $Li_{1.1}Mn_{1.9}O_4$ films was demonstrated to be

independent of deposition method but depended on the film thickness. Optimum performance was obtained with the PLD film deposited for 30 min, which showed almost the same shape of discharge curve between 36 C and 720 C.

Encouraged by the good electrochemical performance and stable crystal structure of $LiFePO_4$, many groups tried to synthesize other poly-anion compounds with similar structures. Thus, Xie et al. [45] fabricated a $LiCoPO_4$ thin film by magnetron sputtering. It showed a (111) preferred orientation up to 600 °C. The Li^+ diffusion coefficient (D_{Li}) in the film declined from 7×10^{-13} cm^2 S^{-1} at 4.71 V to 6×10^{-14} cm^2 S^{-1} at 5 V upon charging. They concluded that the Li ions deintercalation mechanism in $LiCoPO_4$ thin film differed from that in $LiFePO_4$ because the D_{Li} of $LiFePO_4$ showed no significant dependence in the voltage range 3.5–3.7 V. Ma et al. [46] used electrostatic spray deposition (ESD) to prepare $LiMnPO_4$ and $LiFeMnPO_4$ thin films. The particle size of the films was less than 100 nm. $LiFeMnPO_4$ thin films showed two discharge plateaus at 3.9 and 3.4 V, corresponding to the respective reductions of Mn and Fe. Its reversible capacity was higher than that of pure $LiFePO_4$ and $LiMnPO_4$ thin films. Wang et al. [47] fabricated a $Li_3V_2(PO_4)_3$/C thin film via electrostatic spray deposition that demonstrated a reversible capacity of 118 mAh g^{-1} with good capacity retention at the current rate of 1 C, while delivered 80 mAh g^{-1} at 24 C. Tang et al. [48] developed a low-voltage amorphous $LiNiVO_4$ thin film. The useful capacity that may be delivered in practical lithium-ion batteries was about 209 μAh cm^{-2} μm^{-1} between 0.02 and 1.5 V. The charge and discharge curves measured at different current densities were similar. A drop in discharge capacity of 11% was observed as the current density was increased from 50 to 200 μA cm^{-2}, indicating excellent rate capability. Reddy et al. [49–52] investigated the electrochemical performance of $LiNiVO_4$ thin films with different compositions and morphologies. Those with the composition $Li_{1.1}NiVO_4$ exhibited best performance. Their results revealed that the morphologies of the films strongly affected cycling performance. An optimized film exhibited a large reversible capacity of 640 mAh g^{-1}, even after 200 cycles in the range of 0.02–3.0 V, implying that it could be a promising anode for thin-film lithium-ion batteries. Our group employed RF magnetron sputtering to fabricate thin films of $CuWO_4$, Bi_2WO_6 and $LiFe(WO_4)_2$ based on the poly-anion WO_4^{2-} framework [53–55]. The particle size in the $CuWO_4$ thin films was about 20 nm [53]. In electrochemical characterization, two discharge plateaus were observed at 2.5 and 1.6 V, corresponding to the reaction of Cu^{2+}/Cu and of W^{6+}/W^{4+}. The initial reversible capacity of the $CuWO_4$ thin film was about 200 mAh g^{-1}, but it showed fast capacity fading during cycling. The Bi_2WO_6 thin film had a large initial discharge capacity of 133 μAh cm^{-2} μm^{-1} and also exhibited such rapid capacity fading during cycling [54]. The $LiFe(WO_4)_2$ thin film had two discharge plateaus at 3.0 and 1.5 V, corresponding to the reaction of Fe^{3+}/Fe^{2+} and W^{6+}/W^{x+} ($x = 4$ or 5), and delivered a large discharge capacity of 106 μAh cm^{-2} μm^{-1} with good cycling performance [55]. Interestingly, this kind of poly-anion cathode material shows double active-reaction centers involving a change in the valence state of M (M = Cu, Fe, Bi), as well as in W. This feature supports the considerable specific capacity of this kind of cathode material.

3.3. Carbon thin-film electrodes

Carbon-based materials have been commercialized for large-scale lithium ion batteries as intercalation anodes. However, their usage in thin-film lithium batteries is not popular since it is difficult to fabricate carbon-based thin film, and the interface between carbon and the solid-state electrolyte usually is poor. Only a few studies have been completed on thin-film carbon-based anodes. Abe et al. fabricated a highly graphitized carbonaceous thin film by plasma-assisted chemical vapor deposition (PACVD) [56]. Electrochemical characterization indicates the films show similar properties to the graphite electrodes used in common lithium-ion batteries. Lee et al. [57] investigated the electrochemical behavior of the mesophase pitch-carbon thin film. They found that lithium first deintercalated from the graphitized part and then was extracted from the ungraphitized part of the carbon; they concluded that the rate of insertion/extraction response to the graphitized part is faster than that to the ungraphitized part. Hess et al. [58] fabricated graphite multilayer thin films (ten layers with a thickness of 800 nm) and used them as the anodes for Li-ion microbatteries. They present a metal-like conductivity and a resistivity higher than bulk graphite. Their cyclic voltammetry study showed that these thin films exhibit a typical pure graphite behavior. Lu et al. [59] prepared a diamond-like carbon (DLC) thin film by a direct current (DC) magnetron-sputtering method and characterized its electrochemical behavior with lithium. They paid special attention to the effects of the sp^2/sp^3 ratio on the electrochemical properties of such DLC films, finding that a high fraction of sp^2 bonding is preferable for assuring high capacity and long cycling life. Li et al. fabricated highly ordered carbon micro-net films (CMNFs) through patterning and pyrolyzing SU-8 photoresist [60]. They showed stable long-term cycles with a capacity about 100 μAh cm^{-2}. After 100 cycles, the original 3D shape of CMNFs was well preserved, with no evidence of structural collapse and network rupture (Fig. 3a–c). In the presence of pyrolysis temperature gradients, Li^+ insertion mainly is vertical to the cross-section of CMNFs (Fig. 3b and d). In contrast, in the absence of pyrolysis temperature gradients, most Li^+ intercalated or de-intercalated parallel to the cross-section of the CMNF's sides (Fig. 3c and e).

Besides their use in lithium ion batteries, carbon thin films were also utilized in lithium air batteries. Yang et al. [61] fabricated diamond-like carbon thin film and used it as an air electrode in a Li-air battery for the first time. It exhibited high discharge plateaus around 2.7 V, and large reversible-capacity around 2318 mAh g^{-1} at a current density of 220 mA g^{-1} with a capacity loss less than 1.6% per cycle for the first ten cycles. Fig. 4 shows the cross-sectional SEM images of the film during its initial cycle. A flat DLC film (385 nm thick) is observed clearly on Si substrate. After discharge, a 40–60 nm white layer of discharge product formed on the DLC; it consisted of Li_2O_2 and Li_2CO_3, confirmed by the results of Raman spectroscopy, SAED and FTIR. After recharge, the white layer disappeared indicating the film's recovery its former morphology. The sp^3-bonded carbon atoms in DLC thin film seemingly should play a key role in its good electrochemical performance.

4. Thin-film electrode based on conversion reaction

The capacity of thin-film electrode materials based on the traditional insertion/extraction reaction mechanism is limited, as shown in Table 1. Few materials can deliver specific capacities above 200 mAh g^{-1}. Recently, a new kind of electrode reaction-mechanism attracted much attention, viz., the so-called "conversion reaction" mechanism based on the size effect of the nanoparticles. This kind of electrode material normally encompasses a binary-metal compound. The electrochemical reaction equation is represented as follow,

$$MX + nLi^+ + ne^- \leftrightarrow M + Li_nX$$

In discharge process, MX decomposes to form nanosized metal particles that are well dispersed in a Li_nX matrix. In the charging process, MX can be reproduced reversibly. It is a new electrochemical reaction mechanism based on the nanoparticles' size effect. Generally speaking, Li_nX is a relatively stable ionic compound.

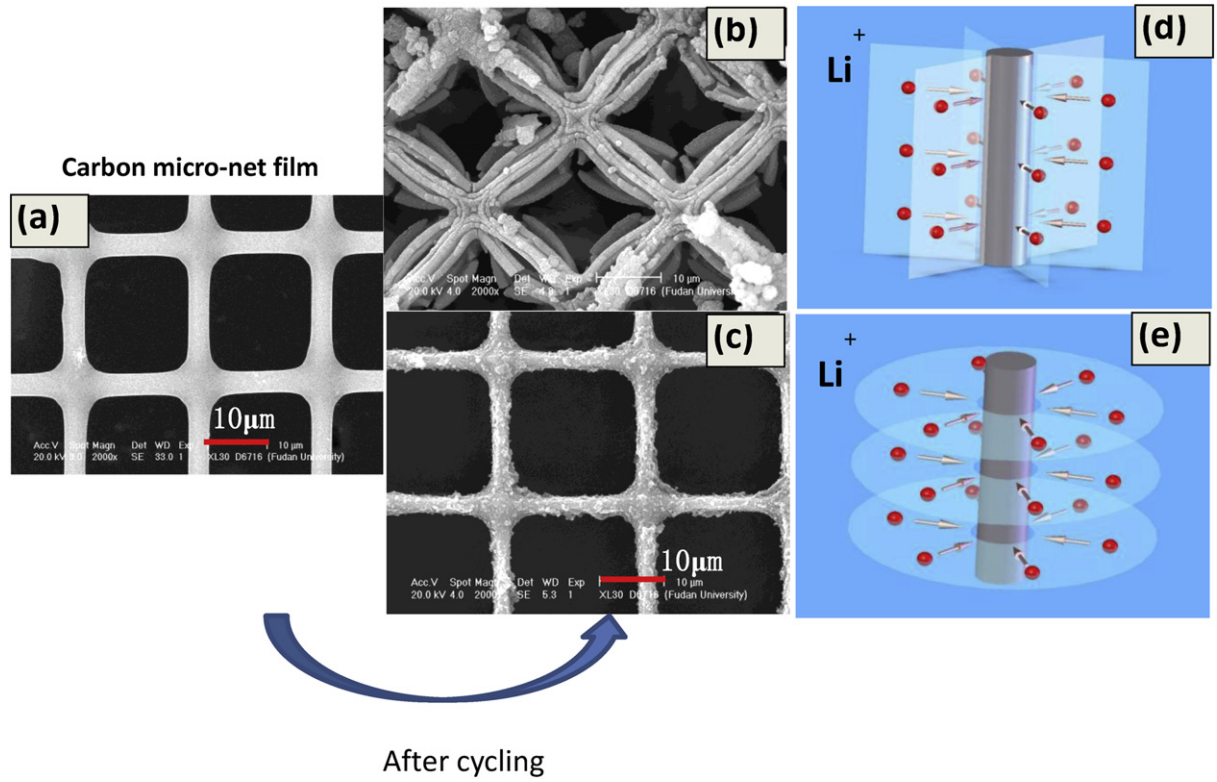

Fig. 3. SEM images of CMNFs (a) after annealing and after the 100th cycle between 0 V and 3 V at a current density of 6 μA cm^{-2} (b) with, and (c) without the pyrolysis temperature gradients. Their corresponding reaction models (d) and (e) of CMNFs with Li^+. Reproduced from Ref. [60].

Li–X bond is difficult to be broken by transition metals to form MX. However, nano-sized metal particles with improved kinetics and thermodynamics could decompose Li_nX by the driving of a certain potential to form MX. The electrode materials based on conversion reactions usually have large reversible capacities [62]. Such thin-film electrodes fabricated via this kind of new mechanism have been widely investigated. The research generally focuses on five systems (Fig. 5): 1. MX; 2. M + Li_nX; 3. MX + Li_nX; 4. MXY; and, 5. MX + Z (M = metal; X, Y=O, F, N, S, P, Se, CO_3, PO_4 and others; Z = nonmetal).

4.1. Metal oxide (MO_x) thin film electrodes

In 2000, Poizot et al. [62] reported that nanosized transition-metal oxides react reversibly with lithium at room temperature. This reaction mechanism existed in many transition metal-oxide systems, such as CoO, Co_3O_4, FeO, and NiO. Later, this mechanism was further confirmed by Obrovac et al. [63] during their investigation of nanosized α-$LiFeO_2$, β-Li_5FeO_4 and CoO powder-electrodes by *in-situ* XRD and Mössbauer measurements. Thin film is a very unique system wherein to study these materials based on the conversion reaction. There are three distinct advantages for these thin-film electrodes. First, they are free from additives and binders, so they offer an unmixed condition within which to investigate a material's intrinsic characteristics. Second, the films are easy to synthesize. Third, they can be deposited on a current collector assuring extensive contact between the active particles and the substrate. The contact is much better than that of powder materials. Li and coworkers [64] fabricated thin-film electrodes of

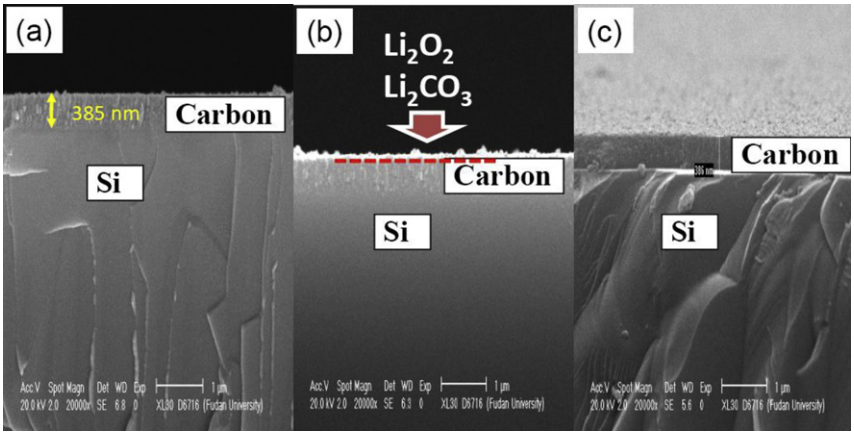

Fig. 4. Cross-sectional SEM images of (a) the as-deposited, (b) discharging to 2.0 V, and (c) charging to 4.5 V DLC thin film electrodes. Reproduced from Ref. [61].

Table 1
Electrochemical performance of thin film electrodes based on intercalation/deintercalation reaction mechanism.

Thin films	Discharge plateau/V	Reversible capacity/mAh g^{-1}
$LiCoO_2$ [9–21]	3.8–4.2	120–170
$LiNiO_2$ [22,23,25]	3.5–4.2	100–130
$LiNiCoO_2$ [24,26,44]	3.7–4.2	100–150
$LiNiMnO_2$ [27]	3.7–4.5	170
$LiMn_2O_4$ [28–34,44]	3.8–4.2	100–140
$LiMn_xNi_{2-x}O_4$ [35]	3.8–4.7	70–100
$LiFePO_4$ [38–44]	3.4–3.5	100–170
$LiCoPO_4$ [45]	4.5–4.8	20
$LiMnPO_4$ [46]	3.6–4.0	8
$LiFeMnPO_4$ [46]	3.2–4.0	60
$Li_3V_2(PO_4)_3$ [47]	3.4–4.0	118
$LiNiVO_4$ [48–52]	0.0–2.0	400–640
$CuWO_4$ [53]	1.0–2.7	140
Bi_2WO_6 [54]	1.0–2.3	93
$LiFe(WO_4)_2$ [55]	1.0–3.0	160
C [56–60]	0.0–0.4	300–500

pseudobinary mischmetal–Fe–O libraries by combinatorial sputtering methods. They proved that doping transition-metal oxides with rare earth metals lowers the working potential of the former, but results in lower reversible capacities. Co_3O_4 thin films synthesized by different technologies exhibited different reaction mechanisms [65–69]. Thus, Co_3O_4 thin films prepared by PLD demonstrated reversible conversion between Co_3O_4 and Co/Li_2O [65–67], while Co_3O_4 thin films prepared by electrolytic deposition were converted into CoO after the initial cycle instead of Co_3O_4 [68,69]. With a Cr_2O_3 thin-film system, Dupont et al. revealed that it had changed into CrO after a full cycle [70]. Analysis of the electrochemical impedance on the Cr_2O_3 thin-film indicated that ohmic polarization, charge-transfer resistance, and diffusion impedance fell significantly during lithiation and rose during delithiation [71]. Differently, MnO, NiO, ZnO, Ta_2O_5 thin films exhibited totally reversible conversion reaction processes due to the regeneration of their initial phases [1,72–74]. This, a nickel-oxide film with monodispersed open macropores yielded a large reversible capacity of 1620 mAh g^{-1} at 1 C current rate and still kept at 990 mAh g^{-1} at 15 C current rate, indicating excellent rate capability [75].

After gaining this understanding of this mechanism further, we are considering whether it could be extended to other metal-oxides. Accordingly, we fabricated SnO_2, Sb_2O_3, In_2O_3 and GeO_2 thin-film electrodes were by PLD and recorded their electrochemical behaviors [76–79]. We found that part of the discharge product Li_2O could be decomposed, generating the metal oxide. Fig. 6 shows the cyclic voltammogram (CV) curves for these as-deposited thin films. The couple of reduction and oxidation peaks, denoted by red circles, never previously was observed in their bulk electrodes, corresponding to the reversible reduction and oxidation of metallic Sn, Sb, In, and Ge. These results challenge the conventional view that the reversible reaction of these metal oxides with lithium is related to the classical alloying process. Although the reduction and oxidation of metals is not fully reversible, nevertheless, it increase the reversible capacity remarkably. The findings suggest that this kind of conversion reactions exists not only in transition metal oxides, but also in main-group metal oxides. (For interpretation of the references to color in this paragraph, the reader is referred to the web version of this article.)

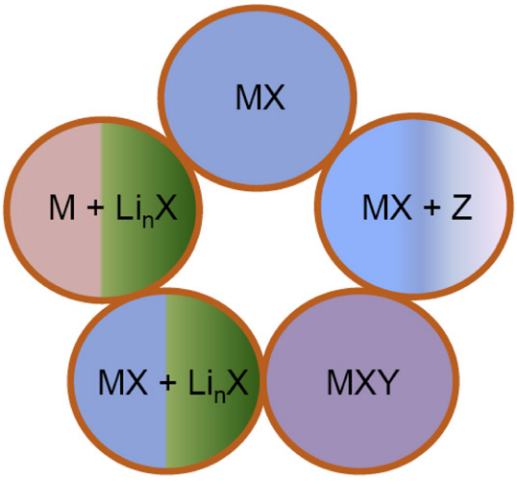

Fig. 5. Scheme for designing thin film electrode materials based on the conversion reaction mechanisms.

4.2. Metal fluoride MF_x thin-film electrodes

Li et al. [80] were the first to propose that conversion-reaction mechanism also existed in metal fluoride. In their study of TiF_3 and VF_3, they found that these two fluorides could be decomposed and reformed reversibly. Their specific capacities were 500–600 mAh g^{-1} with a theoretical voltage of about 3.0 V. Thus, they are promising cathode material for future rechargeable lithium batteries. However, due to the poor electronic conductivity of metal fluoride, polarization during the charge/discharge process was serious. To improve their electronic conductivity, Badway et al. [81,82] prepared a nano-sized FeF_3/C powder electrode by the high energy ball-milling method. Doping with carbon enhanced the electronic conductivity significantly, thereby bettering electrochemical kinetics. A reversible capacity of 200 mAh g^{-1} was recorded in the voltage range of 2.8–3.5 V, corresponding to the Fe^{3+}/Fe^{2+} redox couple. When the FeF_3/C electrode was discharged to 1.5 V, a large plateau was evident between 1.5 and 2.2 V with a capacity of 450 mAh g^{-1}, which was ascribed to the reduction process from Fe^{2+} to Fe^0. This process also was reversible. Another way to weaken the effect of poor electronic conductivity is by fabricating materials into types of thin-films. Thus, Makimura et al. [83,84] prepared FeF_3 thin film by pulsed laser deposition. It showed good reversibility between 1.0 and 3.5 V with a capacity of about 600 mAh g^{-1}. However, the discharge plateaus of FeF_3 thin film were lower than those of FeF_3/C powder electrode; this was because 15% carbon was added in the FeF_3 powder but nothing was added to the thin film. These results indicate the doping a conductive agent might well change the electrochemical kinetics of FeF_3 electrode significantly. Our group prepared CoF_2, NiF_2, MnF_2 and CuF_2 thin-films and probed their electrochemical performances and reaction mechanism with lithium [85–89]. The particle size in the thin films was 20–50 nm. During the discharge process, the transition metal particles (Co, Ni, Mn, Cu) and LiF were formed. During the charge process, CoF_2 showed a different reaction mechanism from other three thin films. Thus, NiF_2, MnF_2 and CuF_2 could be reversibly reproduced after the charge, but CoF was formed, rather than CoF_2 as delithiated product. In the subsequence cycles, the reversible process reflected the transition between CoF and LiF.

4.3. Metal nitride MN_x thin-film electrode

Generally, metal nitrides show low flat charge/discharge plateau close to that of metallic lithium with good reversibility and large capacities. They normally have an antifluorite or Li_3N structure, which are supportive of lithium-ion mobility (ionic conductivity 10^{-2} S cm^{-1}). Bates et al. [90,91] first employed Sn_3N_4 and Zn_3N_2 as anodes for all-solid-state thin film lithium ion batteries. Neudecker et al. [92] explored the relationship between the composition and performance of SnN_x thin film anode in thin-film lithium ion

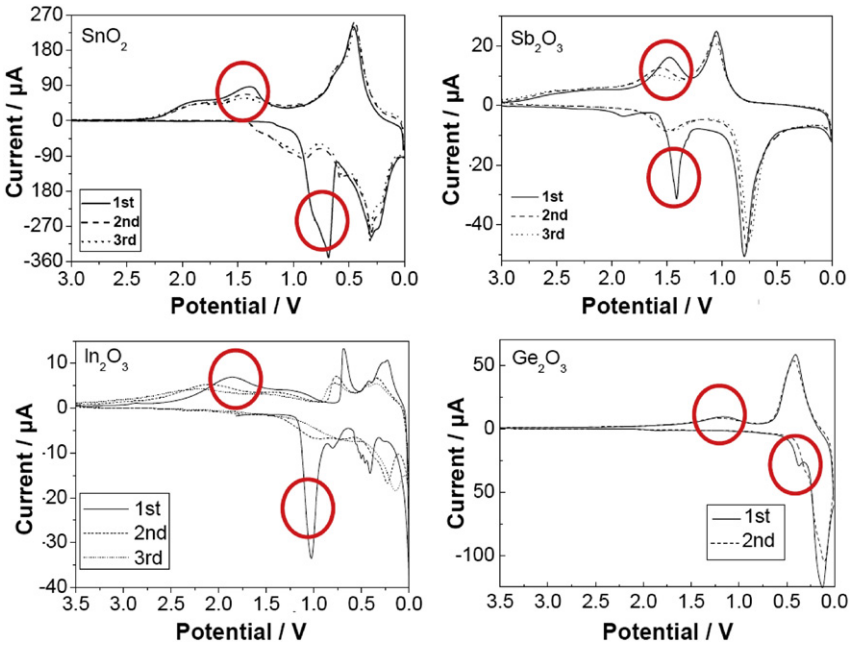

Fig. 6. Cyclic voltammograms for the as-deposited SnO_2, Sb_2O_3, In_2O_3, Ge_2O_3 thin films. The couple of reduction and oxidation peaks shown in red circles correspond to the reversible reduction and oxidation of Sn, Sb, In and Ge. (For interpretation of the references to color in this figure legend, the reader is referred to the web version of this article.) Reproduced from Refs. [76–79].

battery. They found that the capacity increased as the content of N in SnN_x declined. Amatucci et al. detailed the lithium electrochemistry of Zn_3N_2, Ge_3N_4 and Cu_3N [93–95]. They reported that the reaction mechanism of Cu_3N with Li was similar to that of transition metal oxide, i.e., described as reversible conversion between Li_3N and Cu_3N driven by Cu nanoparticles [95]. They also remarked that a few Cu nano-particles were oxidized to copper oxide, attributing this side reaction to the degradation of the liquid electrolyte. Contrary to Cu_3N that displays high reversibility, the initial and reversible capacities of Zn_3N_2 are 1325 and 555 mAh g^{-1}, respectively [93]. A large irreversible capacity exists between the first two cycles. *In-situ* XRD measurements revealed that Zn_3N_2 decomposed to form LiZn and β-Li_3N during the initial discharge, but Zn_3N_2 was not regenerated in the subsequent charge process. The charge products were Zn and LiZnN. Seemingly, β-Li_3N might promote the formation of the ternary compound LiZnN, so entailing a large initial irreversible capacity. As an example of a main-group metal nitride, Ge_3N_4 shows quite different behavior from Zn_3N_2 and Cu_3N [94]. During the first discharge, Ge_3N_4 reacted with Li, generating Li–Ge and also α-Li_3N that proved electrochemical inactive in following cycles. The only reversible reaction in subsequent cycles was the alloying/dealloying reaction between Li and Ge. Furthermore, the conversion efficiency of Ge_3N_4 was very low and the reaction occurred only on the surface of Ge_3N_4 particles.

A series of transition metal-nitride thin films, including VN, CrN, Mn_4N, Fe_3N, Co_3N, Ni_3N, and $Cr_{1-x}Fe_xN$ were fabricated by pulsed laser deposition and magnetron sputtering [96–102]. Except Mn_4N, most transition metal nitride thin film electrodes exhibited good capacity retention ability upon cycling. It is especially noteworthy that although CrN thin film electrode owns a polarization larger than 1 V, the capacity fade of 0.5% per cycle was obtained during 30 charge–discharge cycles, indicating a highly active CrN thin film with good cycle performance [97]. Their electrochemical reaction mechanisms with lithium were investigated. For VN, CrN and Mn_4N thin films [96–98], the reversible reaction occurred between metal nitride and the M/Li_3N composite. Fig. 7 shows the XRD patterns of the CrN thin-film at various potentials during the first cycle; it confirms that CrN can be reversibly regenerated after a full cycle. However, the first cycle of the Fe_3N, Co_3N, and Ni_3N systems were not reversible [99–101]. After discharge, metal particles dispersed in the Li_3N matrix. However, after the charge process, other metal nitrides with lower metal content were generated. The reversible reactions of the subsequent cycles arose from the decomposition/formation reactions of these new-formed metal nitrides while the residual metal particles acted as "active spectators". For example, In Ni_3N system [100], NiN was formed rather than Ni_3N after a full discharge–charge cycle; subsequent cycles involved the reversible reactions between NiN and Ni–Li_3N. Baggetto et al. [103,104] in investigating the reaction mechanism of tin nitride thin-films with lithium recorded a partly reversible conversion-reaction mechanism, evidence for which was based on the end products consisting of octahedrally and tetrahedrally coordinated Sn^{4+} combining with Li_ySn and Li_3N.

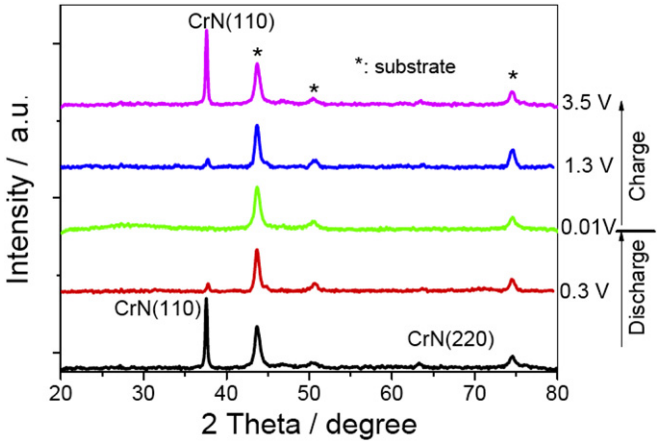

Fig. 7. XRD patterns of CrN thin film at various potentials during the first cycle. Reproduced from Ref. [97].

4.4. Metal selenide MSe_x thin film electrode

Our group for several years has been investigating metal selenide thin films as new electrode materials for lithium-ion batteries. We prepared a series of metal-selenide thin films [105–115], including SnSe, Sb_2Se_3, FeSe, $NiSe_2$, ZnSe, Cu_xSe_y, MnSe and Ag_2Se. They all showed reversible electrochemical behavior but underwent various electrochemical reaction mechanisms with lithium.

The large capacities of tin-based and antimony-based anode materials assured their extensive investigation for lithium-ion batteries [116–119]. Xue et al. prepared SnSe [105,106] and Sb_2Se_3 [107] thin films by pulsed laser deposition and described their electrochemistry with lithium. Their findings show that the electrochemical mechanism of the p-block metal selenide MSe_x (M = Sn, Sb) with Li includes two reversible steps: the decomposition/formation reaction of metal selenide, and the alloying/dealloying reaction of the metal with lithium. Since metal selenide was reproduced after a full cycle involving the latter reaction, the reversibility of the cells was good with a comparatively large specific capacity. InSe thin film [115] also demonstrated the same electrochemical mechanisms as SnSe and Sb_2Se_3.

For the d-block transition metal, FeSe, $NiSe_2$ and MnSe thin films [108–110] were studied. Different from the p-block metal selenide, d-block transition metals did not react with lithium to form Li–M alloy. The electrochemical mechanism of FeSe with lithium simply was the conversion reaction between FeSe and Fe/Li_2Se. The reaction mechanism of $NiSe_2$ system was more complex than that of FeSe. It underwent two intermediate processes involving the formation of the β-NiSe and Ni_3Se_2 phases in the conversion between $NiSe_2$ and Li_2Se. α-MnSe did not decompose completely in the initial discharge process. Instead, a Li-riched phase-Li_xMnSe was formed. In the subsequent charge process, β-MnSe was produced rather than α-MnSe, which was different from the FeSe and $NiSe_2$ systems.

ds-Block transition metal selenides also were investigated. For Ag_2Se [111] and ZnSe [112], the electrochemical reaction mechanisms were similar to that of p-block metal selenides, but they experienced a large capacity loss in the first two cycles and their reversibility was poorer. In the copper–selenide system, there are three kinds of stable phase – $CuSe_2$, CuSe, and Cu_2Se [113]. The morphologies of the three thin films are quite different from each other, as are their electrochemical behaviors (Fig. 8). Their reaction mechanisms with lithium indicated that Cu_2Se could be reproduced after a full cycle, while CuSe and $CuSe_2$ will produce Cu_2Se and Cu_3Se_2 after the discharge and recharge processes.

Besides the above binary metal selenides, a ternary metal selenide – $CuInSe_2$ thin film [114] also was investigated. After discharge, $CuInSe_2$ decomposed and In_3Li_{13}, Cu and Li_2Se were formed. After charge, crystalline Cu_2Se and amorphous In_2Se_3 were produced rather than $CuInSe_2$.

4.5. Metal phosphide (MP_x) thin-film electrode

Nazar et al. firstly suggested MnP_4 as an anode for lithium-ion battery [120]. Since then, metal phosphide has attracted much attention. So far, many metal phosphides have been considered [120–145]. Nazar's group studied MnP_4, FeP_2, CoP_3, and Cu_3P firstly, finding all had versatile electrochemical mechanisms. The reaction of MnP_4 with Li was a one-dimensioned topological conversion reaction between MnP_4 and Li_7MnP_4 [120]. A similar behavior was recorded for FeP_2 [122]. The Fe–P bond was not broken after the initial discharge process and a ternary metastable state compound "Li–Fe–P" was formed. The reversible capacity of FeP_2 was 1250 mAh g^{-1}. The low (ca. 10–15%) irreversibility in the first cycle makes FeP_2 an interesting candidate in the search for new negative electrode materials. For Cu_3P [128], its reaction with Li was a reversible topology replacement one. During discharge, Li_2CuP first was formed and then decomposed, finally forming Li_3P. CoP_3 [124] exhibited an entirely different electrochemical behavior to the above phosphides; the nano-Co particle was not phosphorized during charging process, but acted as a catalyst promoting the conversion between Li_3P and LiP.

Monconduit et al. probed the characteristics of other metal phosphides, such as FeP_x [123], NiP_2 [126], NiP_3 [127], Zn_3P_2 [133], and VP_2 [138]. In studying the FeP_x system ($x = 1, 2, 4$), they found for all of them that the discharge products were Fe and Li_3P, but with different cycling performance. FeP exhibited the best cycle performance (300 mAh g^{-1} was retained after 100 cycles). XRD, Mössbauer spectra, and theoretic calculations confirmed that the electrochemical process encompassed a two-step conversion reaction. A thermodynamically stable intermediate-phase LiFeP was revealed. In characterizing NiP_2, the researchers prepared cubic NiP_2 and monoclinic NiP_2. After discharge, both of them contained Ni and Li_3P. However, NiP_2 with its monoclinic structure showed a better electrochemical performance, exhibiting a large reversible capacity up to 1000 mAh g^{-1}, with a discharge plateau around 0.9 V (vs. Li^+/Li).

Cruz et al. [145] compared the electrochemical properties of electrodeposited Ni_3P thin films, and bulk crystalline Ni_3P. They showed that preparing the material as thin films greatly improved their reversibility and electrochemical performance. Our group described the electrochemical behavior of nano-sized CrP [136], Sn_4P_3 [141] and InP [144] thin films fabricated by pulsed laser deposition. Sn_4P_3 and InP showed a similar electrochemical reaction mechanism with lithium. During the initial discharge phase, Li_3P, Li_xM alloy, and some M (M = Sn, In) were produced. After recharge, Sn_4P_3 and InP were regenerated reversibly (Fig. 9). The CrP system responded differently. CrP was not regenerated after charge. Instead, LiP was formed from the delithiation of Li_3P. Metal Cr did not participate in the following reaction. It was the reversible conversion between Li_3P and LiP.

4.6. M–Li_nX nanocomposite thin film electrode

In 2002, Obrovac and Dahn [146] presented a new type of composite material as the electrode, comprising a transition metal and an inert lithium compound (Li_nX). The Li_2O–M and Li_2S–M (M = Co, Fe) composite synthesized by high-energy ball-milling exhibited considerable electrochemical activity. Its initial discharge capacity was about 600 mAh g^{-1}. This new type of electrode offered two advantages. First, it is a "conversion reaction" system containing lithium and thus, can be compatible with a lithium-free cathode. Second, both the Li_nX compound and metal are stable. These advantages make it safer than metallic lithium as anode for all-solid-state thin-film batteries.

A series of Li_nX–M (X = F, O, S, N; M = Fe, Co, Ni) nanocomposite thin films were developed, and we assessed their electrochemical performance and detailed their reaction mechanisms [147–150]. LiF–Co and LiF–Ni thin films [147,148] were fabricated by pulsed laser deposition, yielding, respectively, reversible capacities of 546 and 313 mAh g^{-1} with the corresponding capacity fading about 0.3% and 0.5% per cycle. A reversible process, of the decomposition and the formation of LiF was revealed during charge and discharge. The results indicate that the transition-metal nanoparticles directly drive the decomposition of the inert LiF. Liao et al. [151] prepared libraries of $[LiF]_{1-x}[Fe]_x$ ($0 < x < 1$) nanocomposite thin-films by combinatorial co-sputtering of lithium fluoride and iron. The relationship between composition and structure was revealed by XRD and Mössbauer spectroscopy. The nanocomposites with a LiF:Fe ratio of 3.0 exhibited the best performance with a capacity of 620 mAh g^{-1} at 70 °C.

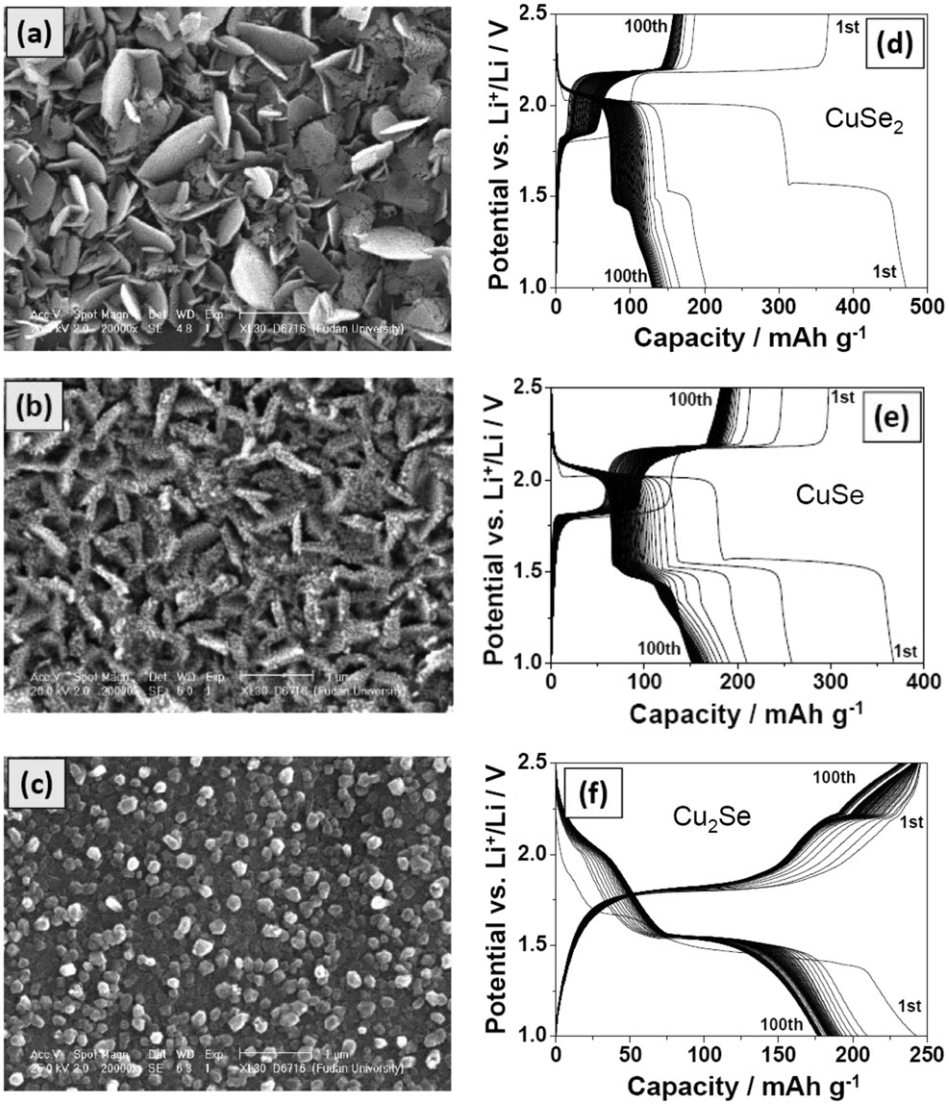

Fig. 8. SEM images of the as-deposited thin films: (a) $CuSe_2$; (b) CuSe; (c) Cu_2Se, and (d), (e) and (f) their respective corresponding galvanostatic curves. All cells are cycled between 1.0 and 2.5 V. Reproduced from Ref. [113].

Li_2S–Co nanocomposite thin film [149] showed different electrochemical reaction mechanisms with LiF–Co. After the initial charge, polycrystalline CoS_2 and S were formed. Subsequent cycles involved the formation/decomposition of Li_2S and the lithium extraction/insertion of CoS_2. The reversible capacity was 819 mAh g^{-1}. But the cycling performance was not satisfied. Only 500 mAh g^{-1} was remained after 22 cycles. The electrochemical behavior of a Li_3N–Co thin film also was studied [150]. In the initial charging process, Co_2N was generated with the decomposition of Li_3N. In the discharging process, a ternary compound, $Li_{2.57}Co_{0.43}N$, was produced with a little Li_3N. Subsequent cycles involved the reversible conversion between $Li_{2.57}Co_{0.43}N$ and Co_2N. The Li_3N–Co thin film displayed a reversible capacity of 400 mAh g^{-1} and better cycling performance than Li_2S–Co thin film mentioned before [149].

The above investigations indicate that a nanosized transition metal can drive the decomposition of LiX (X = F, O, S, N) during electrochemical reactions and that this process is reversible. These findings constitute direct evidence of the decomposition of the inert LiX matrix driven by nano-sized transition metals at room temperature.

Hence, a question emerged whether or not a nonmetal elementary substance could drive the decomposition of LiX matrix. In response, we fabricated a Li_3N–Si nanocomposite thin film [152] by pulsed-laser deposition and recorded its electrochemical behavior. During the initial charge, a capacity of 528 mAh g^{-1} was attained with a voltage plateau around 4.3 V. The product after charging was a polycrystalline hexagonal Si_3N_4. After discharge, a ternary compound Li_5N_3Si was formed similar to $Li_{2.57}Co_{0.43}N$ in the Li_3N–Co system. Subsequent cycles involved the reversible conversion between Li_5N_3Si and Si_3N_4. The Li_3N–Si thin film yielded a large reversible capacity of 700 mAh g^{-1}, but its capacity faded faster than that of the LiX–metal system.

Studies on Li_2Se–Cu_3Se_2 and Li_2Se–Sb_2Se_3 nanocomposite thin films further enlarged the range of the conversion reaction [153,154]. In the initial charge process for the two systems, both of their CV curves showed clear anodic peaks, indicating that both materials could release lithium in the charge process. As shown in Fig. 10, the anodic peak of Li_2Se–Cu_3Se_2 was at 3.8 V, corresponding to the conversion from Cu_3Se_2 to $CuSe_2$. The charged products of Li_2Se–Cu_3Se_2 and Li_2Se–Sb_2Se_3 nanocomposite thin films,

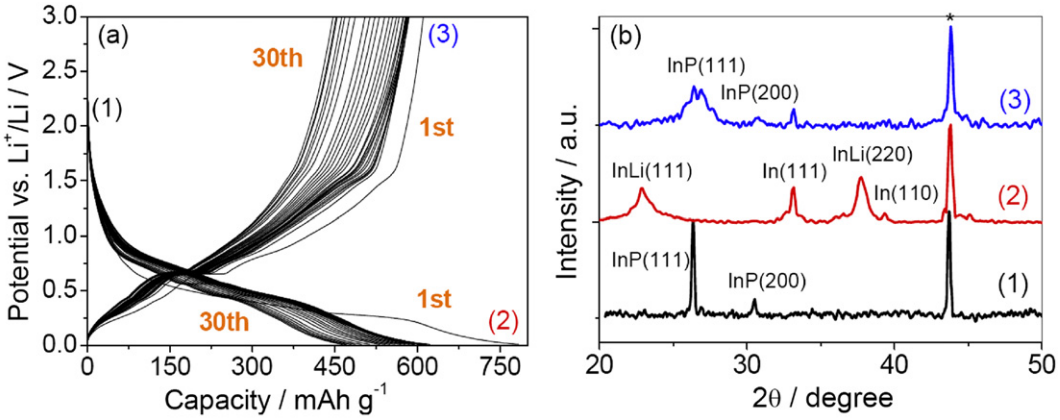

Fig. 9. (a) Charge–discharge cyclic curves at the current density of 10 μA cm^{-2} and (b) *ex situ* XRD patterns of InP thin film at various states during the first cycles. (1) As-deposited; (2) discharging to 0.01 V; (3) charging to 3.0 V. Reproduced from Ref. [144].

respectively, were identified as $CuSe_2$ and Sb_2Se_3. Further investigation denoted that their reversible processes involved the interchange of Cu_2Se/Cu_3Se_2 and Sb_2Se_3/Sb_2Se_5 followed with the decomposition and formation of Li_2Se. These results provided direct experimental evidence supporting the conclusion that the reversible decomposition of Li_2Se was driven by metal selenides; this finding may open a useful route to search for other lithium-storage materials.

4.7. Polynary nanocomposite thin-film electrodes

Each single MX system has its drawbacks. For example, metal fluorides suffer from poor electronic conductivity due to their high ionicity [80–89]; metal oxides normally exhibit poor capacity-retention caused by particle aggregation [64–79], while metal nitride showed serious polarization during charge and discharge [96–98]. To integrate the advantages of single system and compose a more harmonic, neutralized electrochemical system, scientists considered synthesizing polynary systems, such as double anion systems (MX_1X_2) or highly mixed nanocomposites. Amatucci's group [155–159] synthesized a series of metal oxyfluoride by high-energy ball milling, including BiOF, FeOF, AgMoOF, and AgNbOF. They found that the conductivity of the electrode rose remarkably by replacing some of the fluorine with oxygen, resulting in much better electrochemical kinetics. Moreover, the high discharge plateaus of metal fluoride were well retained in metal oxyfluorides. The oxyfluoride exhibits a better electrochemical performance than its corresponding metal oxide or metal fluoride. Xu et al. fabricated thin films of ZnO_xS_{1-x} ($x = 0$, 0.28, 0.67, 1) and studied their electrochemical behavior [154]. A $ZnO_{0.28}S_{0.72}$ thin film showed the best electrochemical performance with a large reversible capacity of 600 mAh g^{-1} and excellent capacity retention (nearly 100% after 40 cycles). The reaction mechanism of $ZnO_{0.28}S_{0.72}$ with lithium was revealed during the cycles. It involved the reversible decomposition of $ZnO_{0.28}S_{0.72}$ (above 0.7 V) and the alloying/dealloying of ZnLi (below 0.7 V). Zhou et al. [161] also investigated the electrochemistry of a V_2ON thin film with lithium; it demonstrated a large reversible capacity of around 800 mAh g^{-1}. Doping oxygen in the

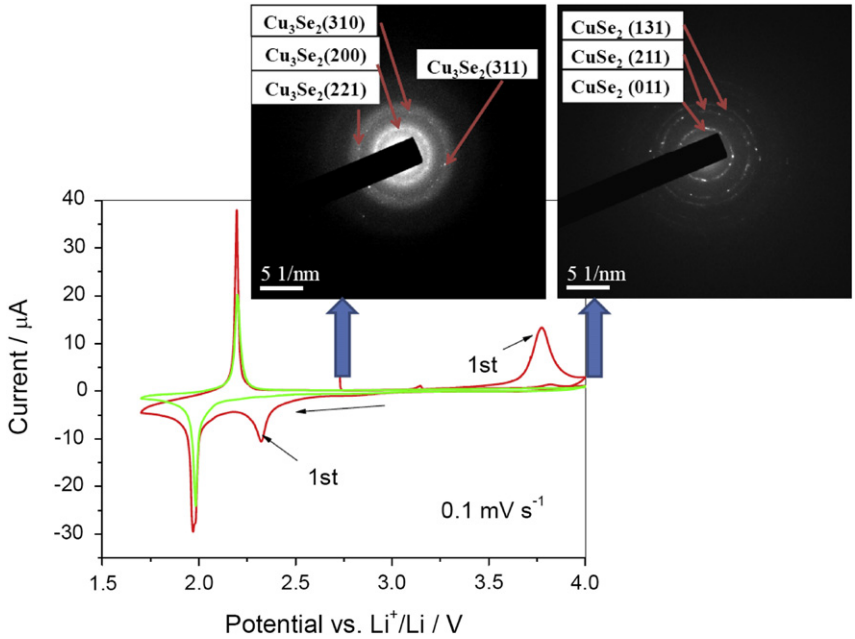

Fig. 10. The first two cyclic voltammograms for the as-deposited Li_2Se–Cu_3Se_2 nanocomposite thin film in a limited voltage ranges of 1.7–4.0 V, and SAED patterns at the as-deposited thin film and after charging to 4.0 V. Reproduced from Ref. [153].

nitrogen site greatly decreased the polarization of the charge/discharge plateaus. The electrochemical reaction mechanism indicated that V_2ON could be reversibly reproduced after a full cycle.

MO–Se (M = Fe, Zn) nanocomposite thin films were developed by Li et al. [162,163]. Fe_2O_3–Se and ZnO–Se films respectively exhibited a reversible capacity of 650 and 505 mAh g^{-1}. Investigations of their electrochemical reaction mechanisms with lithium revealed similar processes. After discharge, highly dispersed M, Li_2O and Li_2Se composite formed. After recharge, MSe were generated with a minority presence of MO_x, indicating that M particle was first to react with Li_2Se to form MSe. It is noteworthy that both nanocomposite thin films exhibited better combination properties than did the corresponding metal oxide or metal selenide thin films.

To further clarify the electrochemical behavior of polynary nanocomposites, we investigated a Cr_2O_3–InP nanocomposite thin film that showed a reversible capacity of 653 mAh g^{-1} [164]. An interesting anion exchange process was revealed. In the first discharge, Cr_2O_3 and InP decomposed yielding the products Cr, LiIn, Li_2O, and Li_3P. In the recharge process, CrP formed, instead of the original Cr_2O_3 as the charging product associated with the decomposition of Li_3P rather than with Li_2O. This reversible alloying/dealloying reaction of In with Li, and the reversible formation and decomposition of CrP were involved in subsequent cycles.

Table 2 presents the reversible capacity and discharge plateau of all these thin film electrodes based on conversion reaction. Evidently, most of these thin-film electrodes exhibit high reversible capacities, i.e., the typical advantage of the "conversion reaction" mechanism. Undoubtedly, they show a different electrochemical behavior from that of the bulk electrodes. However, electrode materials based on the conversion reaction always suffer from high voltage-polarization between charge and discharge, as well as large initial irreversible capacities. Further development is needed on this system to resolve these problems.

Table 2
Electrochemical performance of thin film electrodes based on conversion reaction mechanism.

Thin films	Discharge plateau/V	Reversible capacity/ mAh g^{-1}	Thin films	Discharge plateau/V	Reversible capacity/ mAh g^{-1}
NiO [73,75]	0.0–1.4	700–1000	MnSe [110]	0.0–1.0	349
ZnO [1]	0.0–0.6	500	Ag_2Se [111]	0.0–1.7	505
Ta_2O_5 [74]	0.3–1.0	400	ZnSe [112]	0.0–0.9	426
Co_3O_4 [65–69]	0.3–1.2	640–800	$CuSe_2$ [113]	1.5–2.0	202
MnO [72]	0.0–0.7	472–565	CuSe [113]	1.0–2.0	258
Cr_2O_3 [70,71]	0.0–2.0	600–700	Cu_2Se [113]	1.0–2.2	210
SnO_2 [76]	0.0–1.0	1102	$CuInSe_2$ [114]	0.0–2.0	555
Sb_2O_3 [77]	0.5–1.5	794	InSe [115]	0.0–1.3	400
In_2O_3 [78]	0.0–1.1	883	CrP [136]	0.5–1.2	827
GeO_2 [79]	0.0–0.5	1336	Sn_4P_3 [141]	0.0–0.8	906
FeF_3 [83,84]	0.0–2.9	600	InP [144]	0.0–1.0	620
CoF_2 [85]	0.0–1.7	252	Ni_3P [145]	0.0–1.5	80–150
NiF_2 [86]	0.0–1.8	540	LiF–Co [147]	1.0–3.0	546
MnF_2 [89]	0.0–0.7	530	LiF–Ni [148]	1.0–1.7	313
CuF_2 [87,88]	1.0–3.2	540	LiF–Fe [151]	1.0–2.2	620
VN [96]	0.0–3.0	1156	Li_2S–Co [149]	1.0–2.0	819
CrN [97]	0.0–3.0	1200	Li_3N–Co [150]	1.0–1.3	399
Mn_4N [98]	0.0–0.7	210	Li_3N–Si [152]	0.5–2.0	770
Fe_3N [99]	0.0–1.0	350	Li_2Se–Cu_3Se_2 [153]	1.9–2.1	60
Co_3N [99]	0.0–1.4	400	Li_2Se–Sb_2Se_3 [154]	0.5–2.3	255
Ni_3N [100]	0.0–1.8	410	ZnO_xS_{1-x} [160]	0.0–1.0	600
$Cr_{1-x}Fe_xN$ [101]	0.0–2.0	800–1000	V_2ON [161]	0.0–2.5	800
SnSe [105]	0.0–1.3	583	Fe_2O_3–Se [162]	0.0–2.0	650
Sb_2Se_3 [106]	0.7–1.7	605	ZnO–Se [163]	0.0–1.5	505
FeSe [108]	1.0–2.0	361	Cr_2O_3–InP [164]	0.0–1.7	653
NiSe [109]	0.5–2.2	351			

5. Thin-film electrode based on alloying reaction

Electrode materials based on alloying reactions were the earliest system investigated [165]. Since the 1980s, much research has been directed at lithium alloys aimed at using them as anode materials for lithium-ion batteries. The basic reaction of these materials with lithium is represented simply as follows:

$$M + xLi^+ + xe^- \leftrightarrow Li_xM$$

High capacity and safety are the typical characteristics of alloy materials [166]. However, they inevitably suffer from poor cycle life and high loss of initial capacity, to the resolution of which many efforts have been dedicated. Among the metals having the ability to alloy with lithium, silicon and tin were widely investigated because of their abundance, lack of toxicity, and low cost. Here, we extensively review Si-based and Sn-based thin film electrodes; more reports are available on these two systems than on others.

5.1. Si-based thin films

Silicon is a promising high-capacity anode based on alloying reaction with lithium at a low discharge potential (~370 mV vs. Li^+/Li) [167]. The large theoretical capacity of fully lithiated alloy $Li_{22}Si_5$ is up to 4212 mAh g^{-1}. However, the material's volume expands by 300% during the formation of $Li_{22}Si_5$ phase. This huge volume change engenders the pulverization of the electrochemically active phase, as well degrading contact between the active materials and the current collector. Moreover, the poor conductivity of silicon itself is another serious drawback. Therefore, alleviating this volume effect and increasing conductivity are the two main thrusts in research on Si-based electrodes. Fabricating Si into thin film form is helpful in accommodating the mechanical stresses accompanying Li-ion insertion/extraction. Park et al. [168] fabricated amorphous Si thin-films of 1.5 μm and 3 μm by pulsed laser deposition, finding the capacity of the former was superior to that of the latter. Both films showed good cyclic performances without any abrupt fading in capacity up to the 70th cycle. They attributed their good cyclic performance to strong adhesion and to the high density of the thin films due to the suitable method of fabrication employed. Baggetto et al. [169] investigated the interaction between silicon thin film electrodes and various electrolytes (liquid electrolyte: $LiClO_4$ in propylene carbonate (PC), $LiPF_6$ in ethylene carbonate (EC)/diethyl carbonate (DEC); solid electrolyte: lithium phosphorus oxynitride (LiPON), Li_3PO_4). For liquid electrolytes, they found that the solid–electrolyte-interface (SEI) formation depended on the type of electrolyte used. For solid electrolytes, the deposition of a LiPON electrolyte layer rendered the activation of the interface more complicated compared to that of pure Li_3PO_4. An interlayer material due to partial intermixing was observed after depositing LiPON onto Si. Recently, some studies on patterned Si thin-film afforded interesting results and unique scientific insights [170,171]. Xiao et al. [170] prepared patterned Si thin films on a Cu substrate by electron beam evaporation using three kinds of mesh masks. Those Si patterns below 7–10 μm remained adhered to the Cu substrate during cycling, leading to much better cycling stability and capacity retention than did patterns of other sizes. The gaps

between Si patterns allow stress relaxation and support better cycling stability relative to a continuous film. Baggetto et al. [171] fabricated a honeycomb-structured Si film on planar TiN-covered Si substrate by photoetching. After lithiation, the honeycombs became highly curved (Fig. 11a). The thickness, length and height of the curved wall all increased compared with the starting material. Fig. 11b illustrates the morphological changes during delithiation. Interestingly, the highly curved structure gradually converted back to its original configuration, and the hexagonal honeycombs were recovered finally, with exhibiting only slight deformation.

Lee et al. [172,173] developed M–Si (M = Fe, Co) multi-layer thin films as the anodes for thin-film lithium-ion batteries. The volumetric expansion of silicon is suppressed effectively by imposing a metal layer between the Si layers. These M–Si multi-layer thin films demonstrated excellent capacity retention. Jung et al. [174] successfully coupled the amorphous Si thin films with thin-film $LiMn_2O_4$ cathodes, so fabricating batteries with an output voltage of 3.0–3.8 V and good cyclic durability. Another way to improve the electrochemical performance of Si anode is to alloy Si with active (M_a) or inactive metals (M_i). Dahn et al., and Hatchard et al., developed an economical sputtering system to produce large-size composition-spread libraries encompassing linear- and orthogonal-stoichiometry variations [175,176]. This proved a highly efficient way to investigate materials with different compositions, especially alloys. Fig. 12 shows the contour maps of the Sn/Si- and Al/Si-atomic ratios versus position on the 75 mm × 75 mm $SiSn_xAl_y$ film. Using this technique, a series of Si–M_i (Fe, Mn, Cr + Ni) [177] and Si–M_a (Sn, Zn, Ag, Al) [178–182] alloy thin films were investigated, and the relationship between composition and performance was revealed. Most exhibited better cyclic performance than did pure Si thin-films. In a Si–M_i system, M_i mainly plays the role of the buffer to accommodate volume expansion. A Si–M_a system is more complicated. M_a not only works as a buffer, but participates in the electrochemical reaction with lithium. Interestingly, they exhibit different reaction mechanisms to each other. In the discharge process, amorphous $Li_ySi_{1-x}Sn_x$ was formed in the SiSn system and crystallized $Li_ySi_{1-x}Zn_x$ was formed in the SiZn system, while two phases, $Li_{15}Si_4$ and LiAg, were generated in SiAg system. In charge process, single phase SiSn was generated in SiSn system but Si and Zn nanograins were formed in SiZn system while Si and Ag grains were produced in SiAg system. Our group fabricated nanostructured NiSi thin films by pulsed laser deposition [183]. As shown in Fig. 13, a large reversible capacity of 1220 mAh g^{-1} was obtained with excellent capacity retention. The discharge capacity under 100 mA g^{-1} current rate was slightly lower than the corresponding value under 20 mA g^{-1} current rate, indicating excellent rater performance of NiSi thin films. A new electrochemical-reaction mechanism with lithium was revealed, indicating that Ni could be an "active" participant in the electrochemical reactions of the NiSi alloy with lithium.

5.2. Sn-based thin-films

Among the metal-based electrodes, tin is the most attractive material due to its large specific capacity (~990 mAh g^{-1}) resulting from alloying up to 4.4 Li per Sn. Its working potential is about 0.5 V (vs. Li^+/Li). Wen and Huggins were the pioneers in pursuing lithium-storage materials based on alloying reaction. They demonstrated that Sn reacted with lithium to form a series of Li–Sn diagrams [184]: Li_2Sn_5, LiSn, Li_7Sn_3, Li_5Sn_2, $Li_{13}Sn_5$, Li_7Sn_2, and $Li_{22}Sn_5$. Shortly thereafter much research on Sn-based thin-film anodes appeared in the literature. It falls into two groups, one of them focused on pure Sn thin film. Here, Tamura et al. [185] investigated the anode behavior of a Sn thin film. It exhibited a large initial discharge-capacity of 940 mAh g^{-1}, although the cycle performance was still poor. Chiu et al. [186] fabricated nanocrystalline Sn thin film by RF magnetron sputtering, recording a low loss of capacity in first cycle, which became significant during the first 15–20 cycles; afterward the capacity stabilized. Mesoporous and porous Sn thin films prepared by electrodeposition exhibited high capacities with excellent cyclic performance [187,188]. Multilayered tin thin film [189] delivered a larger capacity and higher coulombic efficiency than smooth tin film because the multilayered structure contains more than 60% open space between adjacent tin layers. Doping with a buffer matrix, such as Sn–Li_2O nanocomposite [190] and Sn/Li_2O multilayer [191] thin film also improves the electrochemical performance of tin thin film.

The other part of this research focused on Sn–M (M = transition metal) alloy materials. Numerous studies have reported on Cu–Sn thin films. Beattie and Dahn [192] prepared Cu–Sn thin films with varying stoichiometries by single-bath, pulsed electrodeposition. They found increasing the Cu content lowered capacities but bettered capacity retention. $Li_{3.8}Sn$ was estimated as the electrochemical reaction product after discharge to 0.001 V, which was corrected to $Li_{3.5}Sn$ (Li_2Sn_7 phase) by Choi et al. [193] after their further investigation on the lithiation reaction of Cu_6Sn_5 thin film.

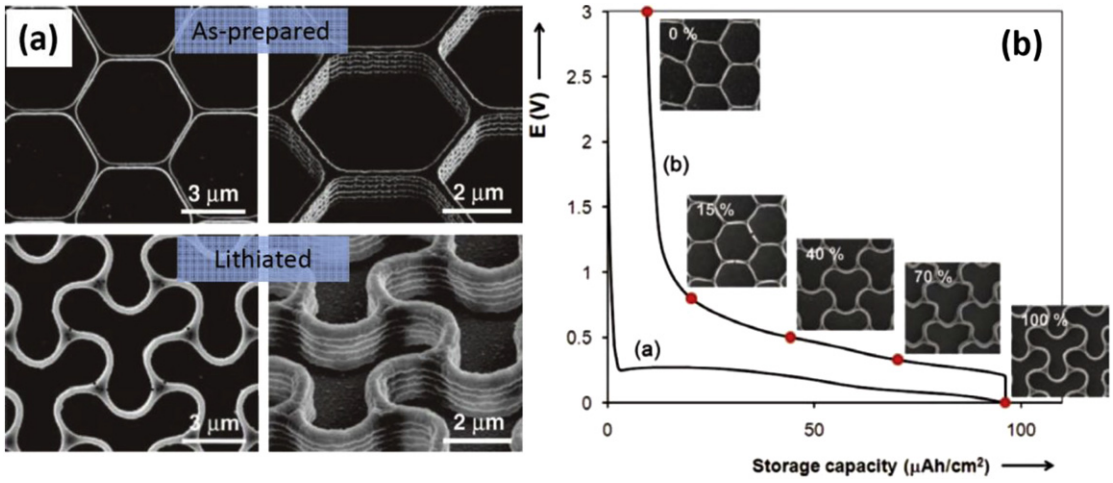

Fig. 11. (a) SEM images of the as-prepared and fully lithiated Si honeycombs; (b) morphological changes of the Si honeycomb structure during delithiation. Reproduced from Ref. [171].

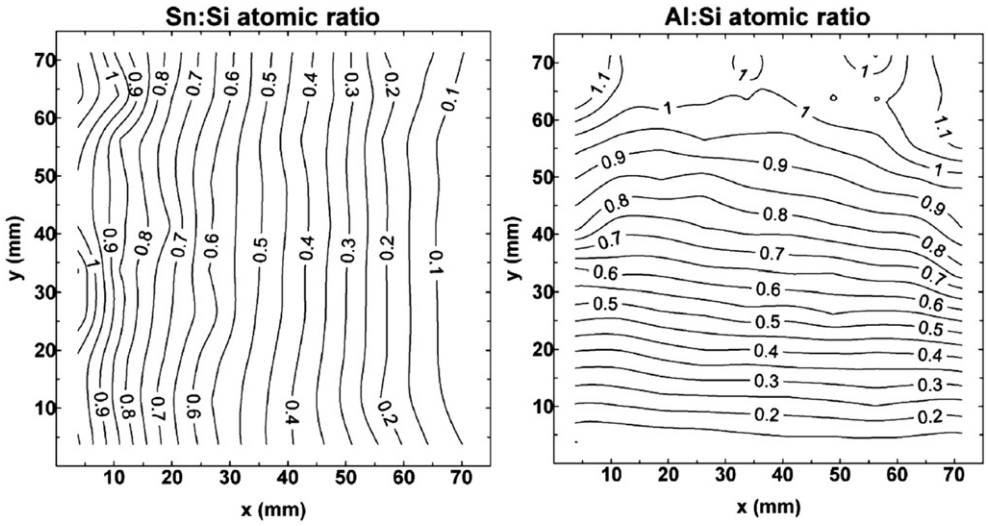

Fig. 12. Contour maps of the Sn/Si and Al/Si atomic ratios versus position on the $SiSn_xAl_y$ film fabricated by a combinatorial sputtering system. Reproduced from Refs. [175,176].

Hu et al. [194] fabricated Sn–Cu alloy with high Cu content by electron-beam evaporation deposition. A discharge capacity of about 200 mAh g^{-1} and coulomb efficiency of 97% remained stable up to the 30th cycle in a voltage window of 0.2–1.5 V versus Li^+/Li. Recently, Thackeray et al. [195] developed microporous Cu_6Sn_5–Sn thin film by electrodeposition that yielded a large reversible capacity of 670 mAh g^{-1}, viz., significantly greater than the capacity achieved previously. Besides Sn–Cu alloy thin film, other Sn-based alloy thin films also were investigated. Kim et al. [196] prepared Ni_3Sn_2 thin films by electron-beam evaporation; they exhibited an excellent reversibility over 500 cycles with a large capacity around 800 mAh g^{-1}. Mukaibo et al. [197] measured the electrochemical performance of Sn–Ni alloy thin film with different Sn/Ni ratios, finding that the film with 62 atom % Sn displayed the best cycle performance. Further investigations [198,199] on this film indicated that the Ni_3Sn_4 phase predominated, resulting in high capacity. Hu et al. [200] developed a Sn–C–Ni composite thin film with a multi-scale structure composed of micro-sized core/shell particles. It exhibited a high-rate capability (472 mA g^{-1} at 12 C) with good capacity retention. Our group fabricated $CrSn_2$ and $CoSn_2$ alloy thin films by pulsed laser deposition [201] recording reversible capacities of 467 mAh g^{-1} and 465 mAh g^{-1}, respectively. After 20 cycles, discharge capacity of about 300 mAh g^{-1} was still kept for both of them. Todd et al. [202] assessed the electrochemical performance of a series of M–Sn (M = Ti, V, Cr, Mn, Fe, Co, Ni, Cu) alloy thin films prepared by magnetron sputtering, finding that the capacity retention is generally better for those with amorphous or highly nanostructured composition. Sn–V alloy seemingly was the best choice among Sn–M alloys. Another group of Sn–M thin film alloys were investigated in which the metal M could alloy with lithium, such as Sn–Al, Sn–Ag, and Sn–Zn. These Sn–M alloy electrodes usually exhibit more complicated electrochemical behavior since the electrochemical active M can react with Li. Shieh et al. [203] detailed the electrochemical properties of AgSn thin-films fabricated by sputtering. In the discharge process, a five-step lithiation reaction was revealed that yielded a large initial discharge capacity

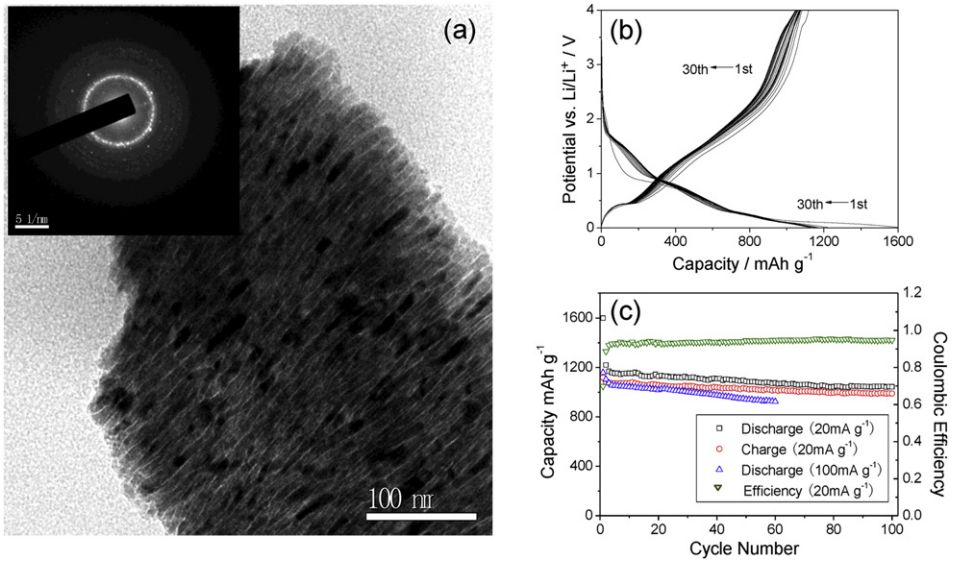

Fig. 13. (a) TEM image and SAED patterns of the nanostructured NiSi thin film; (b) voltage-composition profiles for the nanostructured NiSi thin film/$LiPF_6$/Li cells; (c) cyclic performance and coulombic efficiency of the nanostructured NiSi thin film at a current density of 20 mA g^{-1} and 100 mA g^{-1}. Reproduced from Ref. [183].

of about 900 mAh g^{-1} and a reversible capacity of 400 mAh g^{-1} in 50 cycles. Hu et al. [204–206] used e-beam deposition to fabricate immiscible Al–Sn alloy thin film. The diffusion coefficients of Li^+ in Al–Sn alloy film were 2.1–3.2 $\times$ 10^{-8} cm^2 s^{-1}. The Al-*x* wt % Sn ($40 \leq x \leq 60$) film electrodes showed a good balance among cycling ability, fast Li^+ diffusion, and an acceptable capacity of about 600 mAh g^{-1}. Wang et al. [207] fabricated Sn–Zn alloy film on Cu foil by electroplating; it delivered a reversible capacity of 450 mAh g^{-1} after 50 cycles.

5.3. Other metal thin-films

Germanium is a promising negative electrode for thin film lithium batteries due to its high theoretical capacity (1625 mAh g^{-1}) based on the equilibrium lithium-saturated germanium phase $Li_{22}Ge_5$. Germanium thin film [208] showed stable capacities of 1400 mAh g^{-1} with 60% capacity retention after 50 cycles. It is crystalline in fully lithiated state. Its good performance was attributed to its high surface area and short diffusion lengths. Baggetto et al. [209,210] investigated the lithiation and delithiation process of germanium thin films by *in-situ* X-ray diffraction and absorption spectroscopy; they found that the fully lithiated phase was $Li_{15}Ge_4$ and that during lithiation the first Ge–Ge interatomic distance increased while the Ge–Ge coordination number declined. The opposite was observed for the first Li–Ge interaction. Morales et al. [211] detailed the electrochemical properties of nanocrystalline silver thin films obtained by spray pyrolysis. In the discharge process, at least two Ag–Li alloys formed below 0.2 V, the patterns of which were indexed in the cubic- and tetragonal systems. It could deliver a capacity of 600 mAh g^{-1} in the potential window 0.0–1.0 V. Taillades et al. [212] studied a silver thin-film anode associated with a 5 V $Li_{1.2}Mn_{1.5}Ni_{0.5}O_4$ thin film cathode, obtaining a capacity about 25 μAh cm^{-2} over 1000 cycles at an average working voltage of 4.65 V. Some binary metal alloys were also considered. Thus, Bryngelsson et al. [213] fabricated Cu_2Sb and Cu_9Sb_2 thin films by heating Sb films electrodeposited on Cu substrates. Cu_2Sb showed a stable capacity of 290 mAh g^{-1} while Cu_9Sb_2 was converted to Cu_2Sb during repeated cycling; the capacity of the electrochemically formed Cu_2Sb was 30 mAh g^{-1}. Three separate one-electron oxidation reactions were involved. Trahey et al. [214] studied the effect of electrode dimensionality and morphology on the performance of Cu_2Sb thin film, finding that controlling the active material's surface area, and building internal volume into the electrode structure significantly restrained the capacity fade on cycling. Some ternary alloy compounds also were studied. Kim et al. [215] fabricated Co_2MnAl thin films by DC magnetron-sputtering. The film annealed at 300 °C showed the best electrochemical performance, with a reversible capacity of 430 mAh g^{-1} and good capacity retention. The segregating effect of Co atom played an important role in its electrochemical properties. Hwang et al. [216] generated Si–Ge–Mo alloy thin film by magnetron sputtering. Their $Si_{0.41}Ge_{0.34}Mo_{0.25}$ composite film exhibited excellent electrochemical properties, including a high capacity of 870 mAh g^{-1} over 100 cycles and good coulombic efficiency (ca. 96%). Gnanamuthu et al. [217] investigated the electrochemical performance of Zn–Co–Ni alloy thin film. It delivered an initial discharge capacity of 281 mAh g^{-1} and improved to 650 mAh g^{-1} at the end of 30th cycle with no capacity fading at 0.1 C rate.

Thin film electrodes based on alloying reaction that minimize the effect of volume change normally have superior cycling stability than their corresponding bulk electrodes. Also, they usually have low discharge plateaus and very large reversible capacities (Table 3). The main drawback of these electrodes is the large first-cycle decrement in capacity that is attributes to (a) SEI formation, (b) Li trapping in the host alloy, (c) reaction with oxide impurities, and (d) the aggregation of active particles. These can be reduced by improving the thin films' purity and decreasing the defects in them.

Table 3
Electrochemical performance of thin film electrodes based on alloying reaction mechanism.

Thin films	Discharge plateau/V	Reversible capacity/ mAh g^{-1}
Si [168–171]	0.0–0.3	1000–4000
Co–Si [172]	0.0–0.5	500–2000
Ag–Si [178]	0.0–0.4	1000–2500
Sn–Si [179]	0.0–0.8	1800–3000
Zn–Si [180]	0.0–0.4	1000–3200
Al–Si [182]	0.0–0.4	1000–2400
Ni–Si [183]	0.0–1.5	1220
Sn [185–191]	0.0–0.5	500–850
Cu–Sn [192–195]	0.0–0.8	400–670
Ni–Sn [196–200]	0.0–0.5	450–800
Cr–Sn [201]	0.0–0.5	467
Co–Sn [201]	0.0–0.5	465
Ag–Sn [203]	0.0–0.3	660
Al–Sn [204–206]	0.0–0.5	600
Zn–Sn [207]	0.0–0.5	450
Ge [208–210]	0.0–0.4	1400–1700
Ag [211,212]	0.0–0.3	600
Cu–Sb [213,214]	0.6–1.2	230–290
Co_2MnAl [215]	0.0–1.5	430–600
Si–Ge–Mo [216]	0.0–0.4	870
Zn–Co–Ni [217]	0.0–0.2	300–600

6. Thin-film electrode based on interfacial lithium storage

The concept of interfacial lithium storage was proposed by Maier et al., in 2003 [80,218,219]. In their study on the conversion reaction mechanism of metal fluoride and metal oxide, extra capacity always was obtained reversibly at a low potential range of 0–1.2 V [80,218]. Purportedly, this reversible capacity arose from an interfacial interaction between lithium and the M/LiX matrix, possibly leading to a distinct local charging [218]. The process was clarified by electron injection and ion injection [219,220]. In this model, electron injection occurs at the surface of the non-alloying metal M, while ion injection is likely at the LiX/M surface. This interfacial storage had characteristics resembling those of a capacitor and it was very reversible, unlike Li storage in a passivation layer. First principles calculations and ^6Li NMR results further confirmed the interfacial lithium storage could happen in nanocomposites [221,222] and that at least one monolayer of additional Li can be stored at each interface between LiX and M, thereby resulting in an extra capacity approaching 100 mAh g^{-1}. The interfacial lithium storage was described as a bridge between a capacitor and an electrode behavior. Thin film is an ideal system to investigate the interface due to its flat large surface. Liao et al. [223] studied the interface in ultrathin Al_2O_3/Fe and LiF/Fe multilayers by Mössbauer spectroscopy, where a thin interfacial region existed between Fe layers and the LiF layers. The Li:F ratio was determined to be less than 1 within the interfacial region, suggesting that the 'excess' Li ions were located at the LiF side of the interface and also that the corresponding electrons were delocalized at the Fe side of the interface, i.e., as in good agreement with Maier's interfacial charging theory. Yu et al. [224] fabricated LiF/Ti nanocomposite thin film by pulsed laser deposition. Sloping voltage profiles were found at charge and discharge (Fig. 14c). Compared with pure Ti thin film (Fig. 14a) and LiF thin film (Fig. 14b), the LiF/Ti nanocomposite thin film exhibited an order-of-magnitude larger capacity. Because the LiF phase and Ti phase were unchanged during cycling, the reversible capacity was attributed to the storage of lithium at the grain-boundary regions (Fig. 14d). The typical lithium-storage capacity of

interfacial charging is about 100–300 mAh g^{-1} [225], which is not competitive with other mechanisms of lithium storage in the negative electrode. However, this should be considered especially in nanocomposite thin-film electrodes due to their large surface and abundant grain boundaries.

7. Interface properties of thin-film electrode/electrolyte

Electrode/electrolyte interface is crucially important in the exploration of lithium ion battery suitable for high power and long life operation. Interfacial reactions, which are considered to occur on the nanometric scale, have indeed attracted prime attention in recent years [226,227]. However, for a conventional porous composite electrode consisting of active materials, conductive additives, and polymeric binder, it is difficult to precisely analyze the interfacial reaction due to the complex morphology. Thin-film electrodes deposited by various methods like PLD, sputtering, and ESD consisting of only active material without any additives provide a two-dimensional surface, and hence well-defined interface can be created between electrode and electrolyte, which is particularly helpful to study interfacial reactions. So far, various thin-film electrodes have been prepared to study the interfacial reactions with electrolytes. Abe et al. studied the electrochemical properties of PACVD fabricated graphitized carbonaceous thin films in electrolyte consisting of PC or EC/DEC (1:1 by volume) containing 1 mol L^{-1} $LiClO_4$ [228]. AC impedance spectroscopy showed that charge transfer resistance decreased with decreasing applied rf power, which suggests that highly graphitized carbonaceous thin films with a less-crystallized surface should be ideal electrodes for the fabrication of thin-film batteries. Yamada et al. prepared a $LiMn_2O_4$ thin film by PLD [229]. High activation barrier was found to exist at electrode/electrolyte interface for lithium-ion transfer. The same authors also studied $LiCoO_2$ thin films with different orientations [230]. While charge transfer resistance was strongly influenced by the preferred orientation of $LiCoO_2$ thin film, the activation energy evaluated from the temperature-dependence of Li-ion transfer resistance appeared to be independent of the orientation. Iriyama et al. modified the surface of $LiCoO_2$ thin film electrodes by MgO [231]. CV measurements clearly showed that MgO modification suppresses the increase of resistances caused by repetition of lithium ion insertion/extraction reaction charged up to 4.2 V vs. Li^+/Li. Moreover, the activation energy of lithium ion transfer reaction at $LiCoO_2$/electrolyte interface was also decreased.

The incorporation of solid electrolyte solves the safety and environmental problems generated from volatile and inflammable organic liquid electrolyte for lithium ion battery. Nevertheless, due to the inflexibility of solid electrolyte, the charge transfer resistance at electrode/solid electrolyte interface is even larger than that at electrode/liquid electrolyte interface. Therefore, it is especially important to understand the physical and chemical properties at the electrode/solid electrolyte interface. Iriyama et al. researched the charge transfer resistance at the LiPON/$LiCoO_2$ and LiPON/$LiMn_2O_4$ interface [232,233]. Thermal treatment at 473 K after fabrication of the LiPON/$LiCoO_2$ interface decreased the charge transfer resistance at the interface, and the resistance was further reduced by prolonging the thermal treatment time [232]. On the contrary, this improvement was not observed in case of LiPON/$LiMn_2O_4$ interface [233]. On the other hand, Mn dissolution from $LiMn_2O_4$ thin-film electrode was inhibited due to the formation of LiPON/$LiMn_2O_4$ interface. Okumura et al. revealed that the

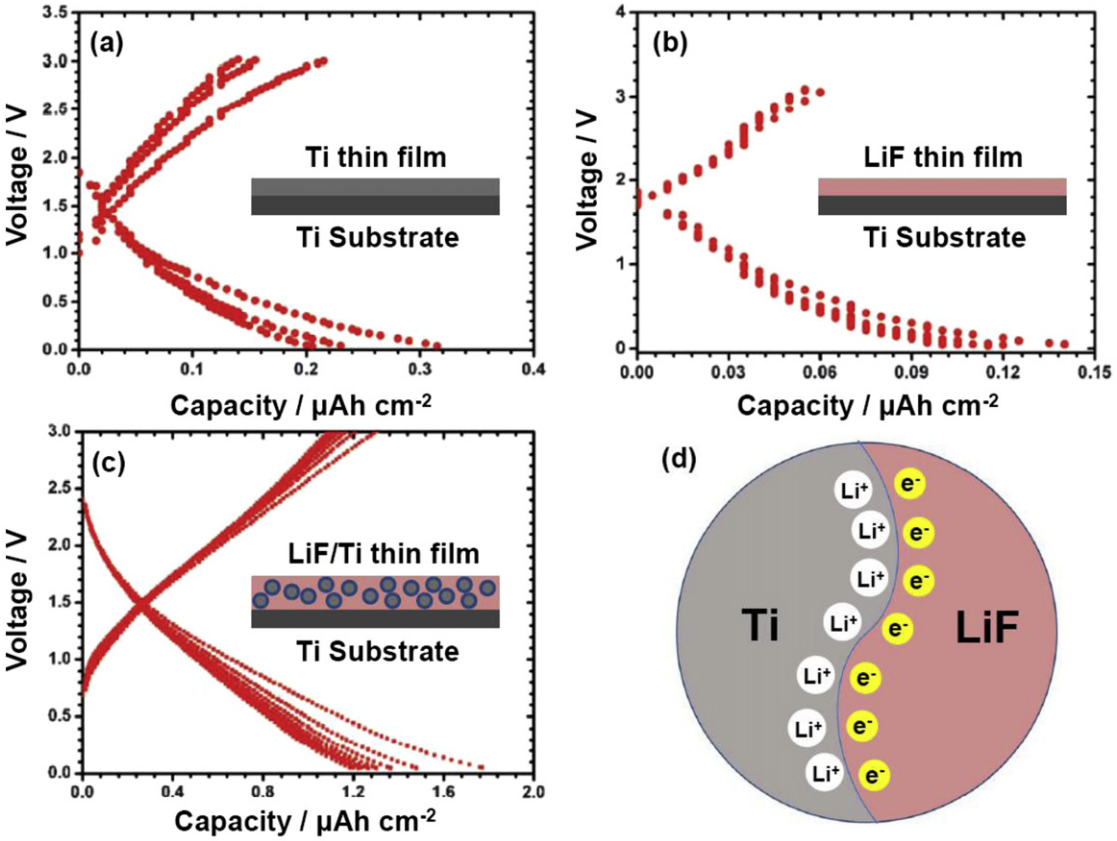

Fig. 14. Voltage composition profiles and illustration of (a) Ti thin film; (b) LiF thin film; (c) LiF/Ti (1:1) thin film on Ti pellet; (d) sketch of interfacial lithium storage. Reproduced from Ref. [224].

introduction of NbO_2 layer relieves the stress at the interface due to the volume change of $LiCoO_2$ during delithiation and then decreased the activation energy for the charge transfer process [234]. By using quantitative electron holography (EH), Yamamoto et al. directly observed the potential distribution resulting from lithium ion diffusion in all-solid-state lithium ion batteries operated within a transmission electron microscope [235]. The results revealed unprecedented detail how the potential due to lithium ions is distributed across a $LiCoO_2$/solid electrolyte interface during charge–discharge reactions. Other electrode/solid electrolyte interfaces, such as $LiCoO_2/Li_7La_3Zr_2O_{12}$ [236] and $LiCoO_2/La_{2/3-x}Li_{3x}TiO_3$ [237], have also been examined.

8. All-solid-state thin film lithium batteries (TFBs)

The development of thin film batteries as miniaturized power sources has been prompted for a variety of applications in micro- and nano-scopic devices. There are two kinds of so-called "thin film lithium/lithium-ion battery" reported so far. The first category employs a polymer or gel film as the electrolyte. Although a battery of less than 0.3 mm thick already was realized [238], it still is far away from the real micro-scale and hence, will not be discussed here. The "thin film lithium/lithium-ion battery" invoked here belongs to another category that appeared about 20 years ago [239]. It has a thickness one order-of-magnitude lower than that of a polymer electrolyte (~10 μm without packaging) and is constructed by techniques used in the microelectronics industry (e.g., sputtering, vacuum evaporation). This battery is aimed at integration with semiconductor devices as a power supply.

In this part, we will review the progress of the thin film lithium/lithium-ion battery. Details of the thin film electrodes that were successfully applied to thin film lithium/lithium-ion battery are summarized and their performance and properties are introduced.

8.1. Thin film cathode

8.1.1. Metal oxides and chalcogenides

The first thin-film cathode incorporated into thin film lithium battery was TiS_2 reported by Kanehori et al. from Hitachi Central Research Laboratory [239,240]. This cathode was deposited by low-pressure chemical vapor deposition (CVD) or plasma-enhanced CVD (PCVD) using $TiCl_4$ and H_2S as the source gas. Films of random- or ordered-(110) crystal orientation were obtained depending on deposition parameters. The films were composed of small plate-like crystals randomly intersecting each other. The discharge capacity of a thin film battery fabricated with PCVD TiS_2 thin film was about 90% of a theoretical one at current densities from 16 to 30 μA cm^{-2}. This represented a significant improvement over the microbattery with a CVD thin film that reached about 55% of its theoretical capacity at 16 μA cm^{-2}, and was attributed to the larger Li^+ diffusion coefficient in the PCVD films.

To generate an amorphous thin film cathode that may benefit the diffusion of isotropic lithium, Meunier et al. fabricated TiO_xS_y thin film via sputtering a TiS_2 target [241]. Oxygen supposedly was present in the target due to the hydrolysis of the TiS_2 while constructing and installing it. The amount of oxygen in the sputtered film depended on the amount of sputtering to which target had been subjected. Microbatteries were constructed using a thin-film cathode with the composition $TiO_{1.5}S_{0.7}$ and had an OCV of 2.6 V. The cells could support relatively high current densities, up to 62 μA cm^{-2}, but the corresponding capacity obtained was 23% of the first discharge capacity obtained at 1 μA cm^{-2}; this loss was attributed to the low diffusion coefficient of the cathode material.

Eveready Battery Company (EBC) was the first to successfully commercialize a thin-film lithium battery with TiS_2 cathode [242]. The cathode film was deposited by radio-frequency (RF) sputtering a TiS_2 target. The deposited film had good stoichiometry ($TiS_{2.09}$) and appeared amorphous to XRD, but SEM showed it was made up of very small crystallites that resulted in a very large active surface area, and was probably one of the reasons that Li^+ could intercalate easily into the cathode thin film. Microbatteries constructed with above TiS_2 cathode film had an OCV near 2.5 V and routinely completed more than 1000 cycles between the limits of 1.4 and 2.8 V, with greater than 90% cathode utilization, at current densities up to 300 μA cm^{-2}. Microbatteries as large as 10 cm^2 also were fabricated and cycled over 1000 times at close to 100% cathodic efficiency.

Other metal sulfides thin films also were investigated [243,244]. A nickel-sulfide thin film developed by Matsumura et al. as a cathode for TFBs delivered a large reversible capacity of 300 mAh g^{-1} in a Ni_3S_2/LISICON/Al–Li all-solid-state cell even after 300 cycles [243]. The cycling performances of the cells were found to be dependent on the Ni_3S_2/LISICON compositions in the cathode mixture, with a cell containing 60 wt.% of Ni_3S_2 exhibiting the most stable reversible capacities. As the depth of the first discharge capacity also influences the cycling properties, Ni_3S_2 consumed during the discharge reaction may play an important role in the nickel reduction mechanism. Iron sulfide thin film incorporated into a Li/CPE/FeS_x cell showed good electrochemical performance in over 650 cycles with 0.06%/cycle capacity loss and 100% Faradaic efficiency at a current density of 50 μA cm^{-2} and 125 °C [244].

Besides metal sulfides, metal oxides and selenides also were successfully incorporated into thin-film lithium batteries. Thus, Julien et al. fabricated InSe thin film by flash evaporation [245]. Their microbattery, with the structure of Li/Li^+–borate glass/InSe, delivered a practical capacity of 30 μAh cm^{-2} at a constant current density of 0.2 μA cm^{-2}. The cell exhibited a voltage versus lithium of 1.45 V. The NTT Corporation, Japan, formulated several thin-film lithium batteries with WO_{3-x}, MnO_{2-x} and MoO_{3-x} cathodes using RF sputtering method [246,247]. Among them, MoO_{3-x} proved to be the best candidate. A microbattery with fairly thick MoO_{3-x} cathode film (~4.66 μm) showed an initial discharge capacity of 398 μA cm^{-2} per unit area and a cycling discharge capacity of 290 μA cm^{-2} per unit area up to 40 cycles, when the discharge constant current density was 10 μA cm^{-2} [247]. The polarization between charge and discharge curves at 20th cycle was only about 0.3 V. Increasing the cathode film's thickness slightly reduced the cathode's utilization at a high discharge current density, but the discharge capacity increased. Some other oxide thin films and oxide mixture thin films, for instance, V_2O_5 [248,249], TiO_2 [250], Fe_2O_3 [251], V_2O_5–WO_3 [252], V_2O_5–TeO_2 [253], V_2O_5–P_2O_5 [253] and MoO_3 [282] also were reported to be successfully integrated into thin film lithium battery by several different groups in the world.

Our group developed an effective method to fabricate silver–V_2O_5 composite thin film using pulsed laser deposition (PLD) [254]. A microbattery, based on 0.5Ag:V_2O_5 thin-film cathode exhibited typical reversible capacities of 42–72 μAh cm^{-2} and the reduction of capacity, was about 1.1% per cycle [255]. Moreover, an improvement also was realized by doping Li into 0.5Ag:V_2O_5 structure [256]. A Li/LiPON/$Li_2Ag_{0.5}V_2O_5$ thin-film microbattery delivered a high discharge capacity of about 60 μAh cm^{-2} after 20th cycles, viz., superior to the corresponding value of Li/LiPON/$Ag_{0.5}V_2O_5$ thin film battery (~42 μAh cm^{-2}). This betterment was attributed to the higher ion-conductivity of $Li_2Ag_{0.5}V_2O_5$ thin film, estimated to be 2.9×10^{-12} cm^2 S^{-1} and two orders-of-magnitude higher than that of an $Ag_{0.5}V_2O_5$ thin film.

8.1.2. Lithium transition metal oxides

Lithium transition-metal oxides were employed in commercial lithium-ion bulk batteries; accordingly, it is worthwhile to explore

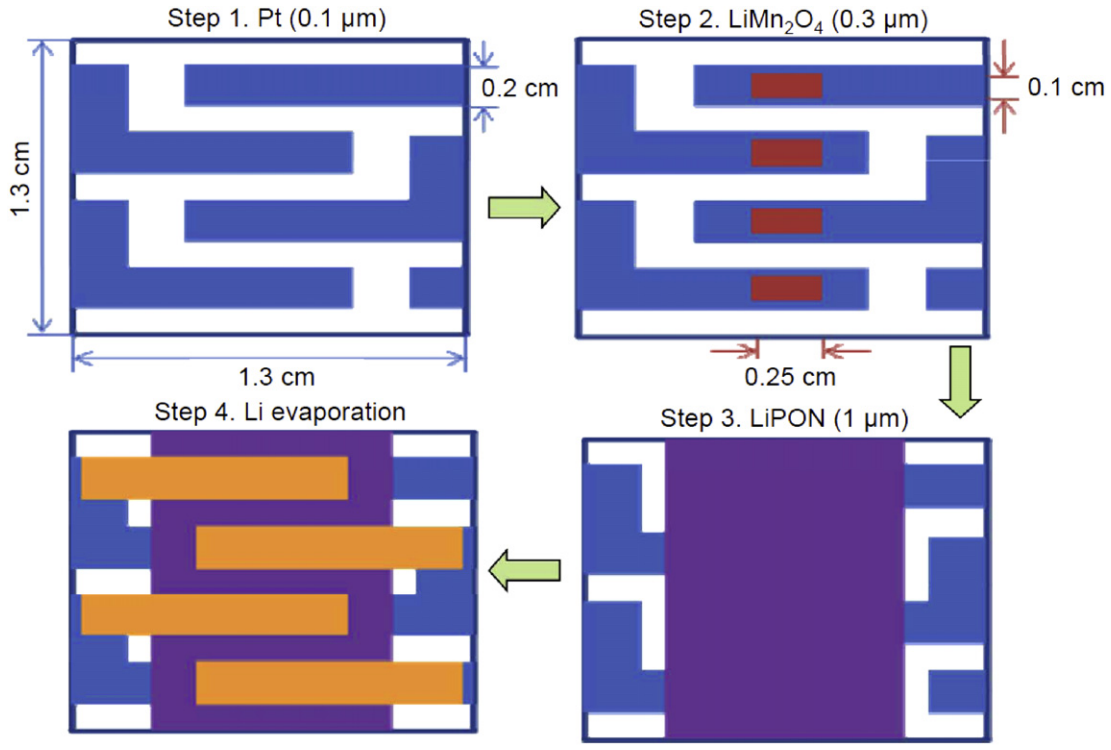

Fig. 15. Plane view of the cell connected in series and its deposition sequences. Reproduced from Ref. [257].

their possible usage in thin film lithium battery. Furthermore, these fully lithiated oxides also could be used with Li-free or Li-ion thin film anodes to produce batteries that can withstand high temperature soldering processes.

Layer structured lithium transition-metal oxides are the most popular cathode materials for commercial lithium-ion batteries. Researchers at Oak Ridge National Laboratory first imported $LiCoO_2$, the most well-known member in the layer oxide family, as the cathode for thin-film lithium batteries [10]. $LiCoO_2$ thin films were deposited by planar RF sputtering of single $LiCoO_2$ targets, and then were subjected to various post-annealing temperatures. Thin film annealed under 700 °C showed superior capacity retention. Losses

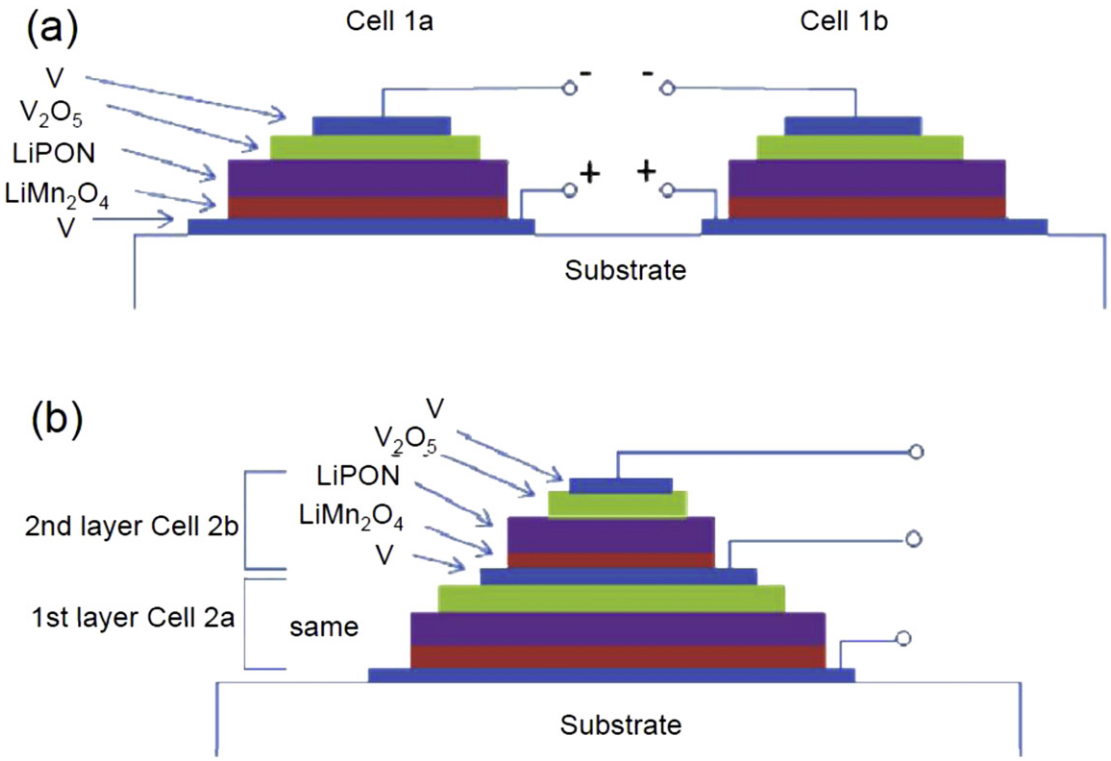

Fig. 16. Schematic drawings of two types of multi-layered thin film batteries: (1) A twin-type battery, and, (2) a stacked-type battery. Reproduced from Ref. [255].

on cycling between 4.2 and 3.8 V at 25 °C ranged from 0.0001%/cycle ($>10^4$ cycles) to 0.002%/cycle for microbatteries with cathodes from 0.05 to 0.5 μm thick. Later, the same group successfully fabricated thin film lithium-ion batteries based on $LiCoO_2$ cathodes [90]. These exciting results intrigued the interest of several research groups worldwide who devoted their attention to $LiCoO_2$-based thin film lithium/lithium ion batteries [257–261]. The Jet Propulsion Laboratory at California Institute of Technology also used RF sputtering to deposit $LiCoO_2$ thin film, but their post-annealing temperature did not exceed 300 °C [257]. Although this partly sacrificed the rate capability of the micro-batteries, the lower operating temperature enabled the integration, via traditional micro-fabrication techniques, of a relatively high-performing thin film microbattery directly onto a Si wafer or a polymer sheet without irreparably damaging the substrate. The NTT Corporation in Japan employed an electron cyclotron resonance (ECR) sputtering method to prepare $LiCoO_2$ thin films [258]. Well-crystallized films were obtained without post-annealing process in a high microwave and RF power range with a low O_2 to Ar ratio. An all-solid-state thin film lithium battery using the $LiCoO_2$ thin film (thickness: 6.2 μm) afforded the relatively large discharge capacity of about 250 μAh cm^{-2} with good cyclability. Moreover, this battery exhibited high discharge capacities of more than 100 μAh cm^{-2} at high current densities of mA cm^{-2} order, indicating excellent rate performance. The feasibility also was demonstrated of preparing thin film batteries on flexible polymer substrate. Kuwata et al. used PLD to fabricate $LiCoO_2$ thin films [259,260], then construct thin film lithium and lithium-ion batteries using these $LiCoO_2$ thin films. *In-situ* photoelectron spectroscopy was utilized to investigate $LiCoO_2$/LiPON interface at different temperatures during the deposition of the LiPON electrolyte [261]. It revealed an intermediate layer composed of some new nitrogen-containing species such as NO_2^-, NO_3^- with a thickness of 10 Å. Liu et al. [15] tested the electrical performance of an Li/LiPON/$LiCoO_2$ all-solid-state lithium battery that they fabricated. The results showed that $LiCoO_2$ thin film annealed at 700 °C exhibited the best performance; a clear discharge plateau between 3.8 and 4.2 V was observed. The specific capacity reached 55.4 μAh cm^{-2} μm^{-1} with good cyclic performance.

Besides $LiCoO_2$, some other layer structure lithium transition metal oxide thin films, such as $Li_x(Mn_yNi_{1-y})_{2-x}O_2$ [262], $LiNiO_2$ [263], $LiNi_{1-x}Co_xO_2$ [23], $LiCo_{0.8}M_{0.2}O_2$ (M = Ni, Zr) [16], $LiNi_{0.8}Co_{0.2}O_2$ [264] and $Li(Ni_{1/4}Mn_{1/2}Co_{1/4})O_2$ [265] reportedly were successfully applied to thin film lithium or lithium ion batteries. Ding et al. [265] fabricated $Li(Ni_{1/4}Mn_{1/2}Co_{1/4})O_2$/LiPON/Li thin film batteries, whose capacity increased along with the cycle number due to the gradual improvement of the interface between cathode and LiPON. A reversible capacity of 30 μAh cm^{-2} μm^{-1} was achieved between 3.0 and 5.0 V.

For spinel-oxide materials, Bellcore constructed a thin film battery with crystalline $LiMn_2O_4$ cathode and glass electrolyte [266] that could be cycled between 3.5 and 4.3 V at current densities up to 70 μA cm^{-2}. Nearly 75% Li was reversibly intercalated into the $LiMn_2O_4$ cathode at 30 μA cm^{-2}. Park et al. fabricated a Li/LiPON/$LiMn_2O_4$ thin film battery [267]. Its discharge occurred at a nearly constant potential of 4.0 V, and the discharge capacity was approximately 48 μAh cm^{-2}, which corresponds to 0.8 Li per mole of Mn_2O_4. The capacity loss was less than 4% after the 100 cycles at a current density of 100 μAh cm^{-2}. By interconnecting 8 unit cells in series, they also achieved a high voltage of approximately 32 V (Fig. 15). Researchers at Oak Ridge National Laboratory reportedly fabricated a thin-film lithium battery with an unannealed, nanocrystalline $Li_xMn_{2-y}O_4$ thin film [268]. Although Li^+ diffusivity was greatly reduced in the disordered material, thereby limiting the power that can be realized with this thin-film cathode, the advantage of this cathode is that it can be used to fabricate thin-film

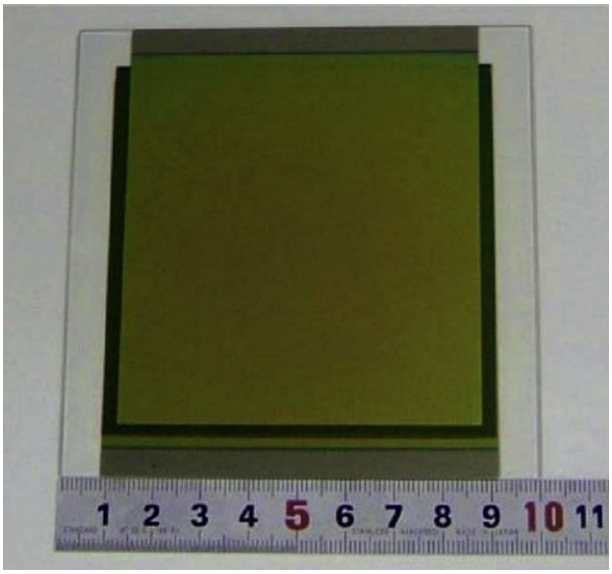

Fig. 17. A photograph of the thin film battery with a 100 mm × 100 mm size in a plane view. Reproduced from Ref. [260].

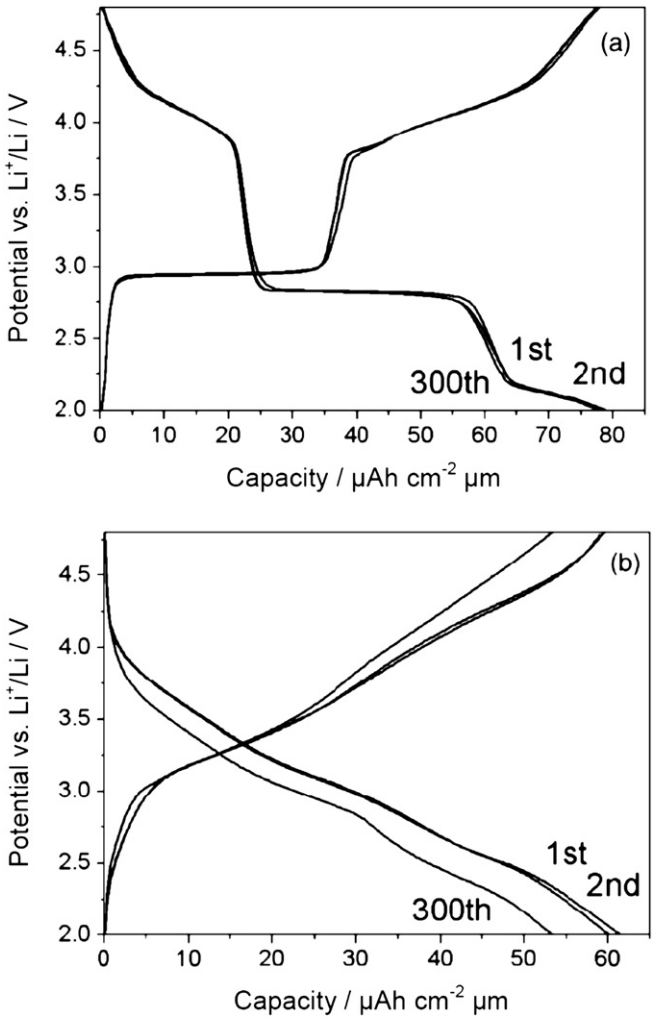

Fig. 18. Voltage composition profiles of (a) $LiMn_2O_4$/LiPON/Li and (b) ZrO_2–$LiMn_2O_4$/LiPON/Li all-solid-state thin-film batteries. Reproduced from Ref. [261].

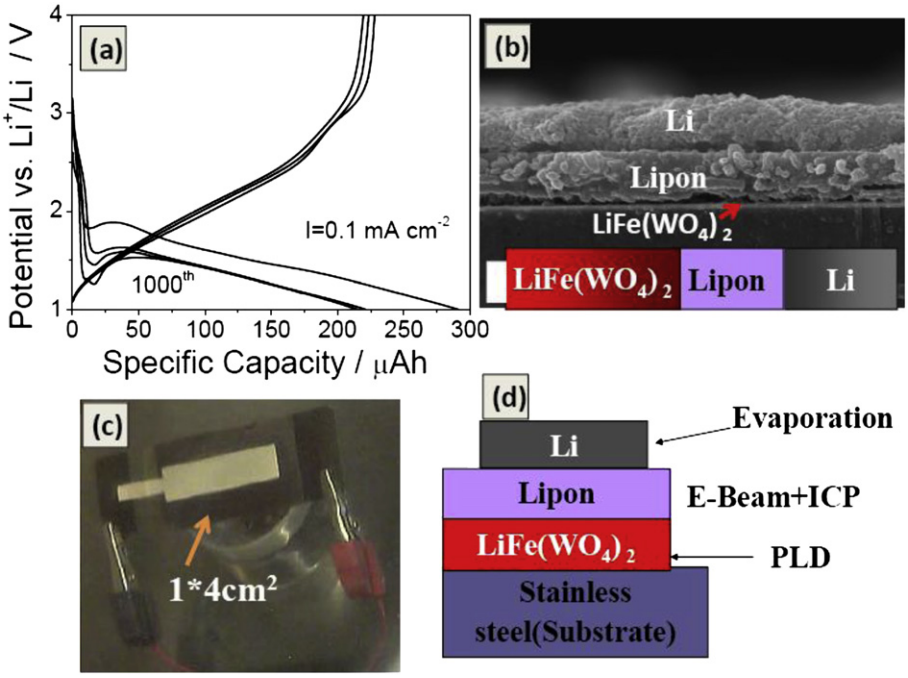

Fig. 19. (a) Discharge and charge curves; (b) cross-sectional SEM images; (c) photograph and (d) structure schematic of the $LiFe(WO_4)_2$/LiPON/Li cell.

batteries on low-temperature substrates or temperature-sensitive devices. Furthermore, these batteries also proved robust, with long cycle lives even when cycled at temperatures up to 100 °C. Baba et al. incorporated $LiMn_2O_4$ thin film into a thin-film lithium-ion battery [269]. Cells with multi-layers (Fig. 16) or large sizes (Fig. 17) also were fabricated [270,271]. Besides these improvements, others were obtained by introducing other transition-metal cations and oxides [35,272,273] or coating them with a metal oxide-retaining layer [272]. Our group fabricated ZrO_2-doped $LiMn_2O_4$ thin film by RF magnetron sputtering [273]. It was found that doping ZrO_2 could effectively lower the particle size of as-deposited thin films An interesting finding emerged during testing of the electrochemical performance of $LiMn_2O_4$/LiPON/Li and $LiMn_2O_4$–ZrO_2/LiPON/Li solid-state batteries, was that ZrO_2 doped $LiMn_2O_4$ showed a sloped discharge plateau from 4.0 to 2.0 V, while the undoped one showed two flat discharge plateaus at 4.0 and 2.8 V, respectively (Fig. 18). It was believed that adding ZrO_2 substantially weakened the change of free energy in annealed LMZO thin film, thereby decreasing the particle size, and changing electrochemical kinetics. The sloped voltage plateau is more suitable for practical application than are distinct plateaus.

8.1.3. Poly-anion compounds

Although several groups worldwide successfully fabricated lithium transition-metal phosphate thin films world [38,39,46], so far, only $LiCoPO_4$ reportedly was realized in thin-film lithium battery [274]. However, that microbattery yielded only a discharge capacity of 11 μAh cm^{-2} at current density of C/15, i.e., lower than the batteries constructed with layered oxide and spinel oxide cathode materials. Therefore, other poly anion compounds must be examined for their possible application in thin film lithium/lithium ion batteries.

Our group recently investigated a series of poly anion compounds and then fabricated thin film lithium batteries based on them. We firstly examined $FePO_4$, which has same PO_4^{3-} poly anion with lithium transition-metal phosphates. With our knowledge of LiPON electrolytes, we prepared nitrogen-doped $FePO_4$ (FePON) thin film; the resulting microbattery showed a higher capacity and better cycling performance than $FePO_4$ microbattery [275]. We ascribed this enhancement to the improved electronic conductivity with nitriding. Afterward, we considered some other compounds based on other poly anions, for example, WO_4^{3-} [53–55]. A typical representative was amorphous $LiFe(WO_4)_2$ thin-film fabricated by RF sputtering [55]. An all-solid-state thin film battery with a new cathode – amorphous $LiFe(WO_4)_2$ was constructed. As shown in Fig. 19, each layer of the TFBs was formed by different techniques. Amorphous $LiFe(WO_4)_2$ was deposited on the substrates by RF sputtering, then a LiPON layer was deposited on $LiFe(WO_4)_2$ thin film by electron-beam evaporation assisted by ICP (Inductively Coupled Plasma) sources. Lastly, Li metal was deposited by thermal evaporation. The electrochemical charge/discharge profiles of a 4 × 4 cm^2 $LiFe(WO_4)_2$/LiPON/Li thin film battery is shown in Fig. 19a. Its reversible capacity was 220 μAh due to the activity of two redox centers (Fe^{3+}/Fe^{2+} and W^{6+}/W^{x+}, where $x = 4$ or 5), with excellent capacity retention in 1000 cycles. It showed much better volume-based rate capacity than did that of $LiCoO_2$ and $LiMn_2O_4$ thin films. Besides its favorable electrode–electrolyte interface, and its unique and outstanding electrochemical performance during long-term cycling proved that $LiFe(WO_4)_2$ thin film was a reliable positive electrode material, and is suitable for application in all-solid-state thin-film lithium battery.

8.2. Thin film anode

Most all-solid-state thin film batteries reportedly use Li metal as anode. However, despite providing a high constant voltage, applications and fabrication processes are limited due to the low melting point of lithium, and its strong reactivity with moisture. This necessitates placing an additional protective multi-layer coating over the lithium anode for fabricating thin-film batteries, which could be costly. Moreover, the choice of electrolytes that are stable enough for use with metallic lithium is very restricted. Therefore, we must develop proper anode film to make a thin film lithium-ion battery.

2Nevertheless, compared with various compounds and the volume of work on cathode films, only limited numbers of compounds have been used in thin film lithium ion batteries. Bates et al. tested several nitrides, such as silicon–tin oxynitrides (SiTON),

Table 4
Thin film lithium and lithium-ion batteries reported in the literature in the last ten years.

Cathode	Anode	Reversible capacity	Current	Voltage range (vs. Li^+/Li) (V)	Year	Ref.
$LiCoO_2$	Li	170 ± 10 mAh g^{-1}	0.1 mA cm^{-2}	3.0–4.4	2002	[14]
$LiNiO_2$	Li	37 μAh cm^{-2} μm^{-1}	10 μA cm^{-2}	2.0–4.2	2002	[23]
$LiNi_{1-x}Co_xO_2$	Li	60.2 μAh cm^{-2} μm^{-1}	10 μA cm^{-2}	2.2–4.2	2002	[253]
$Li_2Ag_{0.5}V_2O_5$	Li	60 μAh cm^{-2} μm^{-1}	7 μA cm^{-2}	1.0–3.5	2003	[244]
$LiCoO_2$	$Si_{0.7}V_{0.3}$	56 μAh cm^{-2} μm^{-1}	N/A	2.0–3.9	2003	[266]
$LiMn_2O_4$	V_2O_5	10 μAh cm^{-2}	2 μA cm^{-2}	0.3–3.5	2003	[260]
$Li_yMn_xNi_{2-x}O_4$	Li	52 μAh cm^{-2} μm^{-1}	30 μA cm^{-2}	3–5.5	2003	[35]
$LiCoPO_4$	Li	11 μAh cm^{-2} μm^{-1}	C/15	3.5–5.2	2003	[263]
$0.5Ag:V_2O_5$	Li	55 μAh cm^{-2} μm^{-1}	7 μA cm^{-2}	1.0–3.5	2004	[243]
$LiCoO_2$	SnO	9.5 μAh cm^{-2}	44 μA cm^{-2}	0.7–3	2004	[249]
$LiFe_{0.5}Mn_{1.5}O_4$	Li	76 mAh g^{-1}	C/10	3.0–4.4	2004	[261]
MoO_3	Li	140 μAh cm^{-2} μm^{-1}	0.7 mA cm^{-2}	1–3.5	2005	[271]
$LiCoO_2$	Li	55.4 μAh cm^{-2} μm^{-1}	10 μA cm^{-2}	3.0–4.2	2005	[15]
$LiMn_2O_4$	V_2O_5	13.75 μAh cm^{-2}	2.5 μA cm^{-2}	0.3–3.5	2005	[260]
$LiCoO_2$	SnO	9.0 μAh cm^{-2}	4.4 μA cm^{-2}	1.0–3.0	2006	[267]
$LiMn_2O_4$	SnO	1.5 μAh cm^{-2}	4.4 μA cm^{-2}	1.0–3.0	2006	[267]
$FePO_4$	Li	21 μAh cm^{-2} μm^{-1}	28 μA cm^{-2}	1.5–4.0	2006	[23]
FePON	Li	63 μAh cm^{-2} μm^{-1}	28 μA cm^{-2}	1.5–4.0	2006	[23]
$LiCo_{0.8}Ni_{0.2}O_2$	Li	56 μAh cm^{-2} μm^{-1}	14 μA cm^{-2}	3.0–4.2	2006	[16]
$LiCo_{0.8}Zr_{0.2}O_2$	Li	50 μAh cm^{-2} μm^{-1}	14 μA cm^{-2}	3.0–4.2	2006	[16]
$LiMn_2O_4$	Nb_2O_5	60 μAh cm^{-2} μm^{-1}	1.95 μA cm^{-2}	0.3–3.5	2007	[265]
$LiCoO_2$	Li	40.3 μAh cm^{-2} μm^{-1}	20 μA cm^{-2}	2.5–4.3	2007	[247]
$Li_xMn_2O_4$	Li	78 μAh cm^{-2} μm^{-1}	28 μA cm^{-2}	2.0–4.8	2007	[262]
$Li_xMn_2O_4$-ZrO_2	Li	53 μAh cm^{-2} μm^{-1}	28 μA cm^{-2}	2.0–4.8	2007	[262]
TiO_2	Li	19 μAh cm^{-2} μm^{-1}	5 μA cm^{-2}	1.0–3.0	2007	[238]
$CuWO_4$	Li	70 μAh cm^{-2} μm^{-1}	14 μA cm^{-2}	1.0–4.0	2008	[53]
$LiFe(WO_4)_2$	Li	56 μAh cm^{-2} μm^{-1}	28 μA cm^{-2}	1.0–4.0	2008	[55]
$LiNi_{0.8}Co_{0.2}O_2$	SnO	19.2 μAh cm^{-2} μm^{-1}	N/A	0–3	2009	[254]
Bi_2WO_6	Li	40 μAh cm^{-2} μm^{-1}	28 μA cm^{-2}	1.5–4.0	2009	[54]
$LiCoO_2$	Li	7.8 μAh cm^{-2}	44 μA cm^{-2}	3.0–4.4	2010	[248]
$Li(Ni_{1/4}Mn_{1/2}Co_{1/3})O_2$	Li	30 μAh cm^{-2} μm^{-1}	N/A	3.0–5.0	2010	[255]

Zn_3N_2 and Sn_3N_4 [90,91]. Among them SiTON performed best [90]. A SiTON/LiPON/$LiCoO_2$ cell sustained 5 mA cm^{-2} between 4.2 and 2.7 V while the anode supplied a reversible discharge capacity of about 340 μAh mg^{-1} or even 450 μAh mg^{-1} after heating at 250 °C in air for 1 h. Testing the long-term cycling stability of a SiTON/LiPON/$LiCoO_2$ cell between 3.93 and 2.7 V demonstrated that the Li_ySiTON's capacity faded only by 0.001% per cycle when charging was stopped as soon as the Li_ySiTON potential reached 0 V vs. Li. Baba et al. fabricated several thin-film lithium ion batteries based on V_2O_5 or Nb_2O_5 anode and $LiMn_2O_4$ cathode [269–271,276]. A multi-layer thin film lithium ion battery also was made from a V_2O_5 anode film [270]. Cells composed of amorphous Nb_2O_5 negative electrode (200 nm thick) and amorphous $Li_2Mn_2O_4$ positive electrode (200 nm), and an amorphous LiPON electrolyte (100 nm),

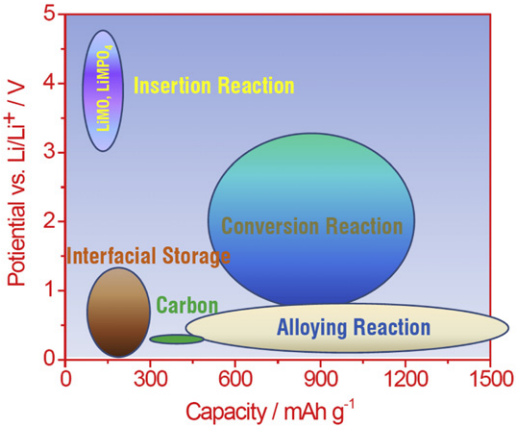

Fig. 20. Comparison of reversible capacity and working potential ranges of the thin film electrodes based on different lithium-storage mechanisms.

showed a large capacity of 600 mAh cm^{-3} [276]. The shape of charge–discharge curve consisted of a two-step for the batteries with the negative electrode thickness more than 200 nm, but that with the thickness of 100 nm was a smooth S-shape curve during 500 cycles. Lee et al. developed a Si–V anode film with the stoichiometry of $Si_{0.7}V_{0.3}$ and constructed a $Si_{0.7}V_{0.3}$/LiPON/$LiCoO_2$ cell [277]. It exhibited excellent cycling stability in cycling between 2.0 and 3.9 V, delivering a stable discharge capacity of ~50 μAh cm^{-1} μm^{-1}; cell performance abruptly deteriorated when the charge cutoff voltage was extended to 4.2 V. Kuwata et al. obtained SnO anode thin film by PLD and constructed several thin-film lithium ion batteries with $LiCoO_2$, $LiNi_{0.8}Co_{0.2}O_2$, and $LiMn_2O_4$ [260,264,278]. To match the Li free cathode, for instance V_2O_5, Baba et al. and Lee et al. fabricated $Li_xV_2O_5$ anode films [279,280]. Baba et al. [279] electrochemically lithiated their as-deposited V_2O_5 thin film to a potential of 0.1 V vs. Li before cell operation whereas Lee et al. [280] thermally evaporated pure Li metal on to the V_2O_5 layer at room temperature in a 10^{-5} mbar vacuum to form their $Li_8V_2O_5$ anode. Both kinds of cells showed a very stable cycling performance. Recently, an *in-situ* SPM study was made on a TiO_2 anode within an all-solid-state thin film lithium battery (TiO_2/LiPON/$LiNi_{1/3}Co_{1/3}Mn_{1/3}O_2$) [281]. Cyclic expansion/contraction was revealed during the Li ion insertion/extraction processes.

Table 4 lists the reports on all-solid-state thin-film lithium and lithium-ion batteries in the last 10 years (2002–2011). Evidently, although layer oxides and spinel oxides are the most popular cathode materials, various kinds of compounds also exhibit attractive performances.

9. Conclusions and outlook

It is important to investigate the underlying relationships between the chemical composition and electrochemical properties of

active material used in lithium batteries. Due to the many advantages on thin-film electrodes over powder-based electrodes, including their high purity, perfect stoichiometry, and freedom from the additives and binders used in the latter, preparing thin film electrodes via versatile deposition technologies undoubtedly has proven the most facile effective way to gain insights into the needed intrinsic properties of lithium-storage materials. In addition, the knowledge obtained from the preferred orientation and anion doping of such thin films by reactive RF sputtering, as well as from patterning thin-film electrodes, could well enrich our understanding of lithium electrochemistry that will be invaluable for lithium storage.

Nanostructured thin-film electrodes exhibit new electrochemical features based on nanometer-size effects and chemical composition. Some of the electrochemical reaction processes could only happen in thin film electrode but not in their bulk one. Obviously, the lithium electrochemistry of thin film electrodes was complex and rich. They involve intercalation/deintercalation reactions, conversion reactions, alloy–dealloying reactions and interface-storage reactions, all of which are highlighted in this review. This comprehensive body of data could enlighten our fundamental understanding of lithium electrochemical reaction mechanisms whilst providing chemists with an effective tool for moving forward this fascinating research field on lithium storage materials for Li-ion battery. The investigations of nanostructured thin films will afford opportunities to study solid-state heterogeneous electrochemistry with polybasic materials on atomic scales for seeking and designing advanced materials having higher store densities of lithium for future rechargeable lithium-ion batteries.

Driven by the constant demands for miniaturizing electronic devices such as complementary metal-oxide semiconductor backups, smart cards, implantable medical devices, and MEMS, great efforts are being directed toward designing and fabricating all-solid-state thin-film lithium batteries with their potential in advantageously offering ultrathin forms, with shape flexibility, lightness, innoxiousness, and non-susceptibility to corrosion and explosion. Together with this, they afford high energy-density, good cycling performance, and they readily withstanding exposure to high temperature and high pressure. In all these features, they differ markedly from the traditional coin-, cylindrical- or prismatic-type cell configurations. The research of all-solid-state thin film lithium batteries (TFBs) is also quite different from that of the traditional lithium batteries, for instance, the interface between the electrode and solid-state electrolyte is quite different from the SEI (Solid Electrolyte Interface) layer in lithium batteries, which has much more impact to the TFB's performance compare with SEI to lithium batteries. In this review, we summarily discussed the many more choices of materials that might serve as the positive and negative thin-film electrodes for thin-film battery components (Fig. 20). Up to now, the best electrode choices for all-solid-state thin film batteries are considered as $LiCoO_2$ ($LiMn_2O_4$ or $LiFeWO_4$) for cathode and Li for anode. During them, in our opinion, $LiFeWO_4$/Li cell is the most promising one due to its considerable performance and low temperature synthesis. The next key issues to be addressed concern the needs for a high-quality electrolyte/electrode interface and the large storage lithium capacity of thin-film electrode; only then we can realize practical high performance all-solid-state rechargeable batteries for daily use.

Acknowledgments

This work was financially supported by 973 Program (No. 2011CB933300) of China and Science & Technology Commission of Shanghai Municipality (08DZ2270500 and 11JC1400500).

References

[1] Z.W. Fu, F. Huang, Y. Zhang, Y.Q. Chu, Q.Z. Qin, J. Electrochem. Soc. 150 (2003) A714.
[2] M. Dawber, C. Lichtensteiger, M. Cantoni, M. Veithen, P. Ghosez, K. Johnston, K.M. Rabe, J.M. Triscone, Phys. Rev. Lett. 95 (2005) 177601.
[3] H.N. Lee, D. Hesse, N. Zakharov, U. Gosele, Science 296 (2002) 2006.
[4] W. Guo, L. Fu, Y. Zhang, K. Zhang, L.Y. Liang, Z.M. Liu, H.T. Cao, X.Q. Pan, Appl. Phys. Lett. 96 (2010) 042113.
[5] D. Swinbanks, Nature 332 (1988) 295.
[6] Y. Yu, C.H. Chen, Y. Shi, Adv. Mater. 19 (2007) 993.
[7] Y.F. Lu, R. Ganguli, C.A. Drewien, M.T. Anderson, C.J. Brinker, W.L. Gong, Y.X. Guo, H. Soyez, B. Dunn, M.H. Huang, J.I. Zink, Nature 389 (1997) 364.
[8] F.K. Shokoohi, J.M. Tarascon, US Pat. Appl. 733 (1991) 224.
[9] M. Antaya, J.R. Dahn, J.S. Preston, E. Rossen, J.N. Reimers, J. Electrochem. Soc. 140 (1993) 575.
[10] B. Wang, J.B. Bates, F.X. Hart, B.C. Sales, R.A. Zuhr, J.D. Robertson, J. Electrochem. Soc. 143 (1996) 3203.
[11] J.B. Bates, N.J. Dudney, B.J. Neudecker, F.X. Hart, H.P. Jun, S.A. Hackney, J. Electrochem. Soc. 147 (2000) 59.
[12] X.J. Zhu, Z.P. Guo, G.D. Du, P. Zhang, H.K. Liu, Surf. Coat. Tech. 204 (2010) 1710.
[13] J. Pracharova, J. Pridal, J. Bludska, I. Jakubec, V. Vorlicek, Z. Malkova, T.D. Makris, R. Giorgi, L. Jastrabik, J. Power Sources 108 (2002) 204.
[14] Y. Jang, N.J. Dudney, D.A. Blom, L.F. Allard, J. Electrochem. Soc. 149 (2002) A1442.
[15] W.Y. Liu, Z.W. Fu, Q.Z. Qin, Chin. J. Chem. Phys. 18 (2005) 1043.
[16] C.L. Li, W.Y. Liu, Z.W. Fu, Chin. J. Chem. Phys. 19 (2006) 493.
[17] C.L. Liao, K.Z. Fung, J. Power Sources 128 (2004) 263.
[18] P.J. Bouwman, B.A. Boukamp, H.J.M. Bouwmeester, H.J. Wondergem, P.H.L. Notten, J. Electrochem. Soc. 148 (2001) A311.
[19] P.J. Bouwman, B.A. Boukamp, H.J.M. Bouwmeester, P.H.L. Notten, J. Electrochem. Soc. 149 (2002) A699.
[20] P.J. Bouwman, B.A. Boukamp, H.J.M. Bouwmeester, P.H.L. Notten, Solid State Ionics 152 (2002) 181.
[21] F. Sauvage, J.M. Tarascon, E. Baudrin, J. Phys. Chem. C 111 (2007) 9624.
[22] X. Lai, D.J. Gao, J. Bi, Y.H. Li, P. Cheng, C.G. Xu, D.M. Lin, J. Alloy Comp. 487 (2009) 130.
[23] H.K. Kim, T.Y. Seong, Y.S. Yoon, Electrochem. Solid-state Lett. 5 (2002) A252.
[24] C.L. Liao, Y.H. Lee, H.C. Yu, K.Z. Fung, Electrochem. Acta 50 (2004) 461.
[25] K.F. Chiu, J. Electrochem. Soc. 151 (2004) A1865.
[26] K.F. Chiu, F.C. Hsu, G.S. Chen, M.K. Wu, J. Electrochem. Soc. 150 (2003) A503.
[27] H. Xia, Y.S. Meng, M.O. Lai, L. Lu, J. Electrochem. Soc. 157 (2010) A348.
[28] K.A. Striebel, C.Z. Deng, S.J. Wen, E.J. Cairns, J. Electrochem. Soc. 143 (1996) 1821.
[29] A. Ueda, J.B. Bates, R.A. Zuhr, Proc. Electrochem. Soc. 98 (1999) 286.
[30] K.F. Chiu, H.H. Hsiao, G.S. Chen, H.L. Liu, J.L. Her, H.C. Lin, J. Electrochem. Soc. 151 (2004) A452.
[31] K.F. Chiu, H.C. Lin, K.M. Lin, C.H. Tsai, J. Electrochem. Soc. 152 (2005) A2058.
[32] C.C. Chen, K.F. Chiu, K.M. Lin, H.C. Lin, Thin Solid Films 517 (2009) 4192.
[33] C.C. Chen, K.F. Chiu, K.M. Lin, H.C. Lin, C.R. Yang, F.M. Wang, M.H. Chiang, J. Electrochem. Soc. 157 (2010) A289.
[34] K.F. Chiu, H.C. Lin, K.M. Lin, C.C. Chen, J. Electrochem. Soc. 153 (2006) A1992.
[35] J.F. Whitacre, W.C. West, B.V. Ratnakumar, J. Electrochem. Soc. 150 (2003) A1676.
[36] A.K. Padhi, K.S. Nanjundaswamy, C. Masquelier, S. Okada, J.B. Goodenough, J. Electrochem. Soc. 144 (1997) 1609.
[37] A.K. Padhi, K.S. Nanjundaswamy, J.B. Goodenough, J. Electrochem. Soc. 144 (1997) 1188.
[38] F. Sauvage, E. Baudrin, M. Morcrette, J.M. Tarascon, Electrochem. Solid-state Lett. 7 (2004) A15.
[39] Y. Iriyama, M. Yokoyama, C. Yada, S.K. Jeong, I. Yamada, T. Abe, M. Inaba, Z. Ogumi, Electrochem. Solid-state Lett. 7 (2004) A340.
[40] C. Yada, Y. Iriyama, S.K. Jeong, T. Abe, M. Inaba, Z. Ogumi, J. Power Sources 146 (2005) 559.
[41] A. Eftekhari, J. Electrochem. Soc. 151 (2004) A1816.
[42] K.F. Chiu, J. Electrochem. Soc. 154 (2007) A129.
[43] K. Tang, X.Q. Yu, J.P. Sun, H. Li, X.J. Huang, Electrochim. Acta 56 (2011) 4869.
[44] T. Matsumura, N. Imanishi, A. Hirano, N. Sonoyama, Y. Takeda, Solid State Ionics 179 (2008) 2011.
[45] J. Xie, N. Imanishi, T. Zhang, A. Hirano, Y. Takeda, O. Yamamoto, J. Power Sources 192 (2009) 689.
[46] J. Ma, Q.Z. Qin, J. Power Sources 148 (2005) 66.
[47] L. Wang, L.C. Zhang, I. Lieberwirth, H.W. Xu, C.H. Chen, Electrochem. Commun. 12 (2010) 52.
[48] S.B. Tang, H. Xia, M.O. Lai, L. Lu, J. Electrochem. Soc. 153 (2006) A875.
[49] M.V. Reddy, C. Wannek, B. Pecquenard, P. Vinatier, A. Levasseur, J. Power Sources 119 (2003) 101.
[50] M.V. Reddy, B. Pecquenard, P. Vinatier, A. Levasseur, Surf. Interface Anal. 39 (2007) 653.
[51] M.V. Reddy, A. Levasseur, J. Electroanal. Chem. 639 (2010) 27.
[52] M.V. Reddy, B. Pecquenard, P. Vinatier, A. Levasseur, J. Phys. Chem. B 110 (2006) 4301.
[53] C.L. Li, Z.W. Fu, Electrochem. Acta 53 (2008) 4293.

[54] C.L. Li, K. Sun, L. Yu, Z.W. Fu, Electrochim. Acta 55 (2009) 6.
[55] C.L. Li, Z.W. Fu, Electrochem. Acta 53 (2008) 6434.
[56] T. Abe, K. Takeda, T. Fukutsuka, Y. Iriyama, M. Inaba, Z. Ogumi, Electrochem. Commun. 4 (2002) 310.
[57] S.J. Lee, M. Nishizawa, I. Uchida, Electrochim. Acta 44 (1999) 2379.
[58] M. Hess, E. Lebraud, A. Levasseur, J. Power Sources 68 (1997) 204.
[59] Z.G. Lu, C.Y. Chung, Diamond Relat. Mater. 17 (2008) 1871.
[60] C.L. Li, Q. Sun, G.Y. Jiang, Z.W. Fu, B.M. Wang, J. Phys. Chem. C 112 (2008) 13782.
[61] Y. Yang, Q. Sun, Y.S. Li, H. Li, Z.W. Fu, J. Electrochem. Soc. 158 (2011) B1211.
[62] P. Poizot, S. Laruelle, S. Grugeon, L. Dupont, J.M. Tarascon, Nature 407 (2000) 496.
[63] M.N. Obrovac, R.A. Dunlap, R.J. Sanderson, J.R. Dahn, J. Electrochem. Soc. 148 (2001) A576.
[64] J. Li, H.M. Dahn, R.J. Sanderson, A.D.W. Todd, J.R. Dahn, J. Electrochem. Soc. 155 (2008) A975.
[65] V. Pralong, J.B. Leriche, B. Beaudoin, E. Naudin, M. Morcrette, J.M. Tarascon, Solid State Ionics 166 (2004) 295.
[66] Y. Wang, Z.W. Fu, Q.Z. Qin, Thin Solid Films 441 (2003) 19.
[67] Z.W. Fu, Y. Wang, Y. Zhang, Q.Z. Qin, Solid State Ionics 170 (2004) 105.
[68] H.C. Liu, S.K. Yen, J. Power Sources 166 (2007) 478.
[69] S.L. Chou, J.Z. Wang, H.K. Liu, S.X. Dou, J. Power Sources 182 (2008) 359.
[70] L. Dupont, S. Grugeon, S. Laruelle, J.M. Tarascon, J. Power Sources 164 (2007) 839.
[71] J.P. Sun, K. Tang, X.Q. Yu, J. Hu, H. Li, X.J. Huang, Solid State Ionics 179 (2008) 2390.
[72] X.Q. Yu, Y. He, J.P. Sun, K. Tang, H. Li, L.Q. Chen, X.J. Huang, Electrochem. Commun. 11 (2009) 791.
[73] Y. Wang, Q.Z. Qin, J. Electrochem. Soc. 149 (2002) A873.
[74] Z.W. Fu, F. Huang, Y.Q. Chu, Y. Zhang, Q.Z. Qin, J. Electrochem. Soc. 150 (2003) A776.
[75] M.S. Wu, Y.P. Lin, Electrochim. Acta 56 (2011) 2068.
[76] M.Z. Xue, Z.W. Fu, Electrochem. Commun. 8 (2006) 1250.
[77] M.Z. Xue, Z.W. Fu, Electrochem. Solid-state Lett. 9 (2006) A468.
[78] Y.N. Zhou, H. Zhang, M.Z. Xue, C.L. Wu, X.J. Wu, Z.W. Fu, J. Power Sources 162 (2006) 1373.
[79] Y.N. Zhou, H. Zhang, C.L. Wu, X.J. Wu, Z.W. Fu, Chin. J. Inorg. Chem. 23 (2007) 1353.
[80] H. Li, G. Richter, J. Maier, Adv. Mater. 15 (2003) 736.
[81] F. Badway, F. Cosandey, N. Pereira, G.G. Amatucci, J. Electrochem. Soc. 150 (2003) A1209.
[82] F. Badway, N. Pereira, F. Cosandey, G.G. Amatucci, J. Electrochem. Soc. 150 (2003) A1318.
[83] Y. Makimura, A. Rougier, J.M. Tarascon, Appl. Surf. Sci. 252 (2006) 4587.
[84] Y. Makimura, A. Rougier, L. Laffont, M. Womes, J.C. Jumas, J.B. Leriche, J.M. Tarascon, Electrochem. Commun. 8 (2006) 1769.
[85] Z.W. Fu, C.L. Li, W.Y. Liu, J. Ma, Y. Wang, Q.Z. Qin, J. Electrochem. Soc. 152 (2005) E50.
[86] H. Zhang, Y.N. Zhou, Q. Sun, Z.W. Fu, Solid State Sci. 10 (2008) 1166.
[87] Y.H. Cui, M.Z. Xue, Y.N. Zhou, S.M. Peng, X.L. Wang, Z.W. Fu, Electrochim. Acta 56 (2011) 2328.
[88] H. Zhang, Y.N. Zhou, X.J. Wu, Z.W. Fu, Acta Phys. Chim. Sin. 24 (2008) 1287.
[89] Y.H. Cui, M.Z. Xue, K. Hu, D. Li, X.L. Wang, W. Su, X.J. Liu, F.M. Meng, Z.W. Fu, J. Inorg. Mater. 25 (2010) 145.
[90] B.J. Neudecker, R.A. Zuhr, J.B. Bates, J. Power Sources 81 (1999) 27.
[91] J.B. Bates, N.J. Dudney, B. Neudecker, A. Ueda, C.D. Evans, Solid State Ionics 135 (2000) 33.
[92] B.J. Neudecker, R.A. Zuhr, Proc. Electrochem. Soc. 24 (2000) 295.
[93] N. Pereira, L.C. Klein, G.G. Amatucci, J. Electrochem. Soc. 149 (2002) A262.
[94] N. Pereira, M. Balasubramanian, L. Dupont, J. McBreen, L.C. Klein, G.G. Amatucci, J. Electrochem. Soc. 150 (2003) A1118.
[95] N. Pereira, L. Dupont, J.M. Tarascon, L.C. Klein, G.G. Amatucci, J. Electrochem. Soc. 150 (2003) A1273.
[96] Q. Sun, Z.W. Fu, Electrochim. Acta 54 (2008) 403.
[97] Q. Sun, Z.W. Fu, Electrochem. Solid-state Lett. 10 (2007) A189.
[98] Y. Wang, W.Y. Liu, Z.W. Fu, Acta Phys. Chim. Sin. 22 (2006) 65.
[99] Z.W. Fu, Y. Wang, X.L. Yue, S.L. Zhao, Q.Z. Qin, J. Phys. Chem. B 108 (2004) 2236.
[100] Y. Wang, Z.W. Fu, X.L. Yue, Q.Z. Qin, J. Electrochem. Soc. 151 (2004) E162.
[101] J. Ma, L. Yu, Z.W. Fu, Electrochim. Acta 51 (2006) 4802.
[102] Q. Sun, Z.W. Fu, Electrochem. Solid-state Lett. 11 (2008) A233.
[103] L. Baggetto, J.C. Jumas, H.T. Hintzen, P.H.L. Notten, Electrochem. Acta 55 (2010) 6617.
[104] L. Baggetto, N.A.M. Verhaegh, R.A.H. Niessen, F. Roozeboom, J.C. Jumas, P.H.L. Notten, J. Electrochem. Soc. 157 (2010) A340.
[105] M.Z. Xue, J. Yao, S.C. Cheng, Z.W. Fu, J. Electrochem. Soc. 153 (2006) A270.
[106] M.Z. Xue, S.C. Cheng, J. Yao, Z.W. Fu, Acta Phys. Chim. Sin. 22 (2006) 383.
[107] M.Z. Xue, Z.W. Fu, J. Alloy Comp. 458 (2008) 351.
[108] M.Z. Xue, Z.W. Fu, Acta Chim. Sin. 65 (2007) 2715.
[109] M.Z. Xue, Z.W. Fu, Electrochem. Commun. 8 (2006) 1855.
[110] M.Z. Xue, Z.W. Fu, Solid State Ionics 178 (2007) 273.
[111] M.Z. Xue, S.C. Cheng, J. Yao, Z.W. Fu, Electrochem. Acta 51 (2006) 3287.
[112] M.Z. Xue, Z.W. Fu, Electrochem. Acta 52 (2006) 988.
[113] M.Z. Xue, Y.N. Zhou, B. Zhang, L. Yu, H. Zhang, Z.W. Fu, J. Electrochem. Soc. 153 (2006) A2262.
[114] M.Z. Xue, Z.W. Fu, Thin Solid Films 516 (2008) 8386.
[115] W.J. Li, Y.N. Zhou, Z.W. Fu, Appl. Surf. Sci. 257 (2011) 2881.
[116] Y. Idota, T. Kubota, A. Matsufuji, Y. Maekawa, T. Miyasaka, Science 276 (1997) 1395.
[117] X.L. Gou, J. Chen, P.W. Shen, Mater. Chem. Phys. 93 (2005) 557.
[118] J.M. Tarascon, M. Morcrette, L. Dupont, Y. Chabre, C. Payen, D. Larcher, V. Pralong, J. Electrochem. Soc. 150 (2003) A732.
[119] S.W. Song, R.P. Reade, E.J. Cairns, J.T. Vaughey, M.M. Thackeray, K.A. Striebel, J. Electrochem. Soc. 151 (2004) A1012.
[120] D.C.S. Souza, V. Pralong, A.J. Jacobson, L.F. Nazar, Science 296 (2002) 2012.
[121] F. Gillot, L. Monconduit, M.L. Doublet, Chem. Mater. 17 (2005) 5817.
[122] D.C.S. Silva, O. Crosnier, G. Ouvrard, J. Greedan, A. Safa-Sefat, L.F. Nazar, Electrochem. Solid-state Lett. 6 (2003) A162.
[123] S. Boyanov, J. Bernardi, F. Gillot, L. Dupont, M. Womes, J.M. Tarascon, L. Monconduit, M.L. Doublet, Chem. Mater. 18 (2006) 3531.
[124] V. Pralong, D.C.S. Souza, K.T. Leung, L.F. Nazar, Electrochem. Commun. 4 (2002) 516.
[125] R. Alcántara, J.L. Tirado, J.C. Jumas, L. Monconduit, J. Olivier-Fourcade, J. Power Sources 109 (2002) 308.
[126] F. Gillot, S. Boyanov, L. Dupont, M.L. Doublet, M. Morcrette, L. Monconduit, J.M. Tarascon, Chem. Mater. 17 (2005) 6327.
[127] S. Boyanov, F. Gillot, L. Monconduit, Ionics 14 (2008) 125.
[128] O. Crosnier, L.F. Nazar, Electrochem. Solid-state Lett. 7 (2004) A187.
[129] M.P. Bichat, T. Politova, J.L. Pascal, F. Favier, L. Monconduit, J. Electrochem. Soc. 151 (2004) A2074.
[130] H. Pfeiffer, F. Tancret, M.P. Bichat, L. Monconduit, F. Favier, T. Brousse, Electrochem. Commun. 6 (2004) 263.
[131] K. Wang, J. Yang, J.Y. Xie, B.F. Wang, Z.S. Wen, Electrochem. Commun. 5 (2003) 480.
[132] M.V.V.M.S. Kishore, U.V. Varadaraju, J. Power Sources 144 (2005) 204.
[133] M.P. Bichat, J.L. Pascal, F. Gillot, F. Favier, Chem. Mater. 17 (2005) 6761.
[134] H. Hwang, M.G. Kim, Y. Kim, S.W. Martin, J.J. Cho, Mater. Chem. 17 (2007) 3161.
[135] C.M. Park, H.J. Sohn, Chem. Mater. 20 (2008) 6319.
[136] J.J. Wu, Z. Sun, Z.W. Fu, Chin. J. Inorg. Chem. 24 (2008) 1761.
[137] Y.U. Kim, B.W. Cho, H.J. Sohn, J. Electrochem. Soc. 152 (2005) A1475.
[138] F. Gillot, M. Ménétrier, E. Bekaert, L. Dupont, M. Morcrette, L. Monconduit, J.M. Tarascon, J. Power Sources 172 (2007) 877.
[139] Y.U. Kim, C.K. Lee, J.J. Sohn, T. Kang, J. Electrochem. Soc. 151 (2004) A933.
[140] B. León, J.I. Corredor, J.L. Tirado, C.P. Vicente, J. Electrochem. Soc. 153 (2006) A1829.
[141] J.J. Wu, Z.W. Fu, J. Electrochem. Soc. 156 (2009) A22.
[142] Y. Kim, H. Hwang, C.S. Yoon, M.G. Kim, J. Cho, Adv. Mater. 19 (2007) 92.
[143] H. Hwang, M.G. Kim, J. Cho, J. Phys. Chem. C 111 (2007) 1186.
[144] Y.H. Cui, M.Z. Xue, X.L. Wang, K. Hu, Z.W. Fu, Electrochem. Commun. 11 (2009) 1045.
[145] M. Cruz, J. Morales, L. Sanchez, J. Santos-Pena, F. Martin, J. Power Sources 171 (2007) 870.
[146] M.N. Obrovac, J.R. Dahn, Electrochem. Solid-state Lett. 5 (2002) A70.
[147] Y.N. Zhou, W.Y. Liu, M.Z. Xue, L. Yu, C.L. Wu, X.J. Wu, Z.W. Fu, Electrochem. Solid-state Lett. 9 (2006) A147.
[148] Y.N. Zhou, C.L. Wu, H. Zhang, X.J. Wu, Z.W. Fu, Acta Phys. Chim. Sin. 22 (2006) 1111.
[149] Y.N. Zhou, C.L. Wu, H. Zhang, X.J. Wu, Z.W. Fu, Electrochem. Acta 52 (2007) 3130.
[150] Y.N. Zhou, H. Zhang, X.J. Wu, Z.W. Fu, Electrochem. Solid-state Lett. 11 (2008) A51.
[151] P. Liao, B.L. MacDonald, R.A. Dunlap, J.R. Dahn, Chem. Mater. 20 (2008) 454.
[152] Y.N. Zhou, X.J. Wu, Z.W. Fu, J. Electrochem. Soc. 156 (2009) A425.
[153] L. Yu, Z.W. Fu, Electrochem. Solid-state Lett. 10 (2007) A146.
[154] L. Yu, J. Chen, Z.W. Fu, Electrochem. Acta 55 (2010) 1258.
[155] M. Bervas, L.C. Klein, G.G. Amatucci, J. Electrochem. Soc. 151 (2006) A159.
[156] N. Pereira, F. Badway, M. Wartelsky, S. Gunn, G.G. Amatucci, J. Electrochem. Soc. 156 (2009) A407.
[157] W. Tong, G.G. Amatucci, Electrochem. Solid-state Lett. 12 (2009) A219.
[158] W. Tong, W.S. Yoon, N.M. Hagh, G.G. Amatucci, Chem. Mater. 21 (2009) 2139.
[159] W. Tong, W.S. Yoon, G.G. Amatucci, J. Power Sources 195 (2010) 6831.
[160] H. Xu, Y.N. Zhou, F. Lu, Z.W. Fu, J. Electrochem. Soc. 158 (2011) A285.
[161] Y.N. Zhou, C. Liu, H.J. Chen, L. Zhang, W.J. Li, Z.W. Fu, Electrochem. Acta 56 (2011) 5532.
[162] W.J. Li, Y.N. Zhou, Z.W. Fu, Electrochem. Acta 55 (2010) 8680.
[163] Y.N. Zhou, W.J. Li, Z.W. Fu, Electrochem. Acta 59 (2012) 435.
[164] W.J. Li, Y.N. Zhou, Z.W. Fu, J. Electrochem. Soc. 157 (2010) A957.
[165] A.N. Dey, J. Electrochem. Soc. 118 (1971) 1547.
[166] C.M. Park, J.H. Kim, H. Kim, H.J. Sohn, Chem. Soc. Rev. 39 (2010) 3115.
[167] B.A. Boukamp, G.C. Lesh, R.A. Huggins, J. Electrochem. Soc. 128 (1981) 725.
[168] M.S. Park, G.X. Wang, H.K. Liu, S.X. Dou, Electrochim. Acta 51 (2006) 5246.
[169] L. Baggetto, R.A.H. Niessen, P.H.L. Notten, Electrochim. Acta 54 (2009) 5937.
[170] X. Xiao, P. Liu, M.W. Verbrugge, H. Haftbaradaran, H. Gao, J. Power Sources 196 (2011) 1409.
[171] L. Baggetto, D. Danilov, P.H.L. Notten, Adv. Mater. 23 (2011) 1563.
[172] Y.L. Kim, H.Y. Lee, S.W. Jang, S.H. Lim, S.J. Lee, H.K. Baik, Y.S. Yoon, S.M. Lee, Electrochim. Acta 48 (2003) 2593.
[173] J.B. Kim, H.Y. Lee, K.S. Lee, S.H. Lim, S.M. Lee, Electrochem. Commun. 5 (2003) 544.

[174] H. Jung, M. Park, S.H. Han, H. Lim, S.K. Joo, Solid State Commun. 125 (2003) 387.
[175] J.R. Dahn, S. Trussler, T.D. Hatchard, A. Bonakdarpour, J.R. Mueller-Neuhaus, K.C. Hewitt, M. Fleischauer, Chem. Mater. 14 (2002) 3519.
[176] T.D. Hatchard, J.R. Dahn, S. Trussler, M. Fleischauer, A. Bonakdarpur, J.R. Mueller-Neuhaus, K.C. Hewitt, Thin Solid Films 443 (2003) 144.
[177] M.D. Fleischauer, J.M. Topple, J.R. Dahn, Electrochem. Solid-state Lett. 8 (2005) A137.
[178] T.D. Hatchard, J.R. Dahn, J. Electrochem. Soc. 152 (2005) A1445.
[179] T.D. Hatchard, J.R. Dahn, J. Electrochem. Soc. 151 (2004) A1628.
[180] T.D. Hatchard, M.N. Obrovac, J.R. Dahn, J. Electrochem. Soc. 152 (2005) A2335.
[181] T.D. Hatchard, M.N. Obrovac, J.R. Dahn, J. Electrochem. Soc. 153 (2006) A282.
[182] M.D. Fleischauer, M.N. Obrovac, J.R. Dahn, J. Electrochem. Soc. 155 (2008) A851.
[183] Y.N. Zhou, W.J. Li, H.J. Chen, C. Liu, L. Zhang, Z.W. Fu, Electrochem. Commun. 13 (2011) 546.
[184] C.J. Wen, R.A. Huggins, J. Electrochem. Soc. 128 (1981) 1181.
[185] N. Tamura, R. Ohshita, M. Fujimoto, S. Fujitani, M. Kamino, I. Yonezu, J. Power Sources 107 (2002) 48.
[186] K.F. Chiu, H.C. Lin, K.M. Lin, T.Y. Lin, D.T. Shieh, J. Electrochem. Soc. 153 (2006) A920.
[187] A.H. Whitehead, J.M. Elliott, J.R. Owen, G.S. Attard, Chem. Commun. 4 (1999) 331.
[188] H. Morimoto, S. Tobishima, H. Negishi, J. Power Sources 146 (2005) 469.
[189] R. Kim, D. Nam, H. Kwon, J. Power Sources 195 (2010) 5067.
[190] C.F. Li, W.H. Ho, C.S. Jiang, C.C. Lai, M.J. Wang, S.K. Yen, J. Power Sources 196 (2010) 768.
[191] J.J. Lee, S.H. Kim, S.H. Jee, Y.S. Yoon, W.I. Cho, S.J. Yoon, J.W. Choi, S.C. Nam, J. Power Sources 178 (2008) 434.
[192] S.D. Beattie, J.R. Dahn, J. Electrochem. Soc. 150 (2003) A894.
[193] W. Choi, J.Y. Lee, H.S. Lim, Electrochem. Commun. 6 (2004) 816.
[194] R.Z. Hu, Y. Zhang, M. Zhu, Electrochim. Acta 53 (2008) 3377.
[195] L. Trahey, J.T. Vaughey, H.H. Kung, M.M. Thackeray, J. Electrochem. Soc. 156 (2009) A385.
[196] Y.L. Kim, H.Y. Lee, S.W. Jang, S.J. Lee, H.K. Baik, Y.S. Yoon, Y.S. Park, S.M. Lee, Solid State Ionics 160 (2003) 235.
[197] H. Mukaibo, T. Sumi, T. Yokoshima, T. Momma, T. Osaka, Electrochem. Solid-state Lett. 6 (2003) A218.
[198] H. Mukaibo, T. Momma, T. Osaka, J. Power Sources 146 (2005) 457.
[199] H. Mukaibo, T. Momma, M. Mohamedi, T. Osaka, J. Electrochem. Soc. 152 (2005) A560.
[200] R.Z. Hu, H. Liu, M.Q. Zeng, H. Wang, M. Zhu, J. Mater. Chem. 21 (2011) 4629.
[201] M.Z. Xue, Z.W. Fu, Solid State Ionics 177 (2006) 1501.
[202] A.D.W. Todd, R.E. Mar, J.R. Dahn, J. Electrochem. Soc. 153 (2006) A1998.
[203] D.T. Shieh, J.T. Yin, K. Yamamoto, M. Wada, S. Tanase, T. Sakai, J. Electrochem. Soc. 153 (2006) A106.
[204] R.Z. Hu, L. Zhang, X. Liu, M.Q. Zeng, M. Zhu, Electrochem. Commun. 10 (2008) 1109.
[205] R.Z. Hu, Q. Shi, H. Wang, M.Q. Zeng, M. Zhu, J. Phys. Chem. C 113 (2009) 18953.
[206] R.Z. Hu, M.Q. Zeng, C.Y.V. Li, M. Zhu, J. Power Sources 188 (2009) 268.
[207] L.B. Wang, S. Kitamura, T. Sonoda, K. Obata, S. Tanase, T. Sakai, J. Electrochem. Soc. 150 (2003) A1346.
[208] J. Graetz, C.C. Ahn, R. Yazami, B. Fultz, J. Electrochem. Soc. 151 (2004) A698.
[209] L. Baggetto, P.H.L. Notten, J. Electrochem. Soc. 156 (2009) A169.
[210] L. Baggetto, E.J.M. Hensen, P.H.L. Notten, Electrochim. Acta 55 (2010) 7074.
[211] J. Morales, L. Sanchez, F. Martin, J.R. Ramos-Barrado, M. Sanchez, J. Electrochem. Soc. 151 (2004) A151.
[212] G. Taillades, J. Sarradin, J. Power Sources 125 (2004) 199.
[213] H. Bryngelsson, J. Eskhult, L. Nyholm, K. Edstrom, Electrochim. Acta 53 (2008) 7226.
[214] L. Trahey, H.H. Kung, M.M. Thackeray, J.T. Vaughey, Eur. J. Inorg. Chem. 26 (2011) 3984.
[215] H.S. Kim, H.S. Ahnn, J.H. Kim, J.H. Park, Y.K. Sun, C.S. Yoon, J. Electrochem. Soc. 157 (2010) A636.
[216] C.M. Hwang, J.W. Park, Electrochim. Acta 56 (2011) 6737.
[217] R.M. Gnanamuthu, C.W. Lee, J. Alloys Comp. 509 (2011) 8933.
[218] J. Jamnik, J. Maier, Phys. Chem. Chem. Phys. 5 (2003) 5215.
[219] P. Balaya, H. Li, L. Kienle, J. Maier, Adv. Funct. Mater. 13 (2003) 621.
[220] J. Maier, Nat. Mater. 4 (2005) 805.
[221] Y.F. Zhukovskii, P. Balaya, E.A. Kotomin, J. Maier, Phys. Rev. Lett. 96 (2006) 058302.
[222] E. Bekaert, P. Balaya, S. Murugavel, J. Maier, M. Menetrier, Chem. Mater. 21 (2009) 856.
[223] P. Liao, R.A. Dunlap, J.R. Dahn, J. Phys. Condens. Matter 20 (2008) 055203.
[224] X.Q. Yu, J.P. Sun, K. Tang, H. Li, X.J. Huang, L. Dupont, J. Maier, Phys. Chem. Chem. Phys. 11 (2009) 9479.
[225] C.X. Zu, H. Li, Energy Environ. Sci. 4 (2011) 2614.
[226] D. Aurbach, B. Markovsky, G. Salitra, E. Markecich, Y. Talyossef, M. Koltypin, L. Nazar, B. Ellis, D. Kovacheva, J. Power Sources 165 (2007) 491.
[227] Z. Ogumi, Electrochemistry 78 (2010) 319.
[228] T. Abe, K. Takeda, T. Fukutsuka, Y. Iriyama, Z. Ogumi, J. Electrochem. Soc. 151 (2004) C694.
[229] I. Yamada, T. Abe, Y. Iriyama, Z. Ogumi, Electrochem. Commun. 5 (2003) 502.
[230] I. Yamada, Y. Iriyama, T. Abe, Z. Ogumi, J. Power Sources 172 (2007) 933.
[231] Y. Iriyama, H. Kurita, I. Yamada, T. Abe, Z. Ogumi, J. Power Sources 137 (2004) 111.
[232] Y. Iriyama, T. Kako, C. Yada, T. Abe, Z. Ogumi, J. Power Sources 146 (2005) 745.
[233] Y. Iriyama, K. Nishimoto, C. Yada, T. Abe, Z. Ogumi, K. Kikuchi, J. Electrochem. Soc. 153 (2006) A821.
[234] T. Okumura, T. Nakatsutsumi, T. Ina, Y. Orikasa, H. Arai, T. Fukutsuka, Y. Iriyama, T. Uruga, H. Tanida, Y. Uchimoto, Z. Ogumi, J. Mater. Chem. 21 (2011) 10051.
[235] K. Yamamoto, Y. Iriyama, T. Asaka, T. Hirayama, H. Fujita, C.A.J. Fisher, K. Nonaka, Y. Sugita, Z. Ogumi, Angew. Chem. Int. Ed. 49 (2010) 4414.
[236] K.H. Kim, Y. Iriyama, K. Yamamoto, S. Kumazaki, T. Asaka, K. Tanabe, C.A.J. Fisher, T. Hirayama, R. Murugan, Z. Ogumi, J. Power Sources 196 (2011) 764.
[237] K. Kishida, N. Wada, H. Adachi, K. Tanaka, H. Inui, C. Yada, Y. Iriyama, Z. Ogumi, Acta Materia 55 (2007) 4713.
[238] K. Murata, S. Izuchi, Y. Yoshihisa, Electrochim. Acta 45 (2000) 1501.
[239] K. Kanehori, K. Matsumoto, K. Miyauchi, T. Kudo, Solid State Ionics 9 (1983) 1445.
[240] K. Kanehori, Y. Ito, F. Kirino, K. Miyauchi, T. Kudo, Solid State Ionics 18 (1986) 818.
[241] G. Meunier, R. Dormoy, A. Levasseur, Mater. Sci. Eng. B 3 (1989) 19.
[242] S.D. Jones, J.R. Akridge, J. Power Sources 54 (1995) 63.
[243] T. Matsumura, K. Nakano, R. Kanno, A. Hirano, N. Imanishi, Y. Takeda, J. Power Sources 174 (2007) 632.
[244] V. Yufit, K. Freedman, M. Nathan, L. Burstein, D. Golodnitsky, E. Peled, Electrochim. Acta 50 (2004) 417.
[245] C. Julien, A. Khelfa, N. Benramdane, J.P. Guesdon, P. Dzwonkowski, I. Samaras, M. Balkanski, Mater. Sci. Eng. B 23 (1994) 105.
[246] J. Yamaki, H. Ohtsuka, T. Shodai, Solid State Ionics 86 (1996) 1279.
[247] H. Ohtsuka, Y. Sakurai, Solid State Ionics 144 (2001) 59.
[248] J.B. Bates, N.J. Dudney, G.R. Gruzalski, R.A. Zuhr, A. Choudhury, C.F. Luck, J.D. Robertson, J. Power Sources 43 (1993) 103.
[249] E.J. Jeon, Y.W. Shin, S.C. Nam, W.I. Cho, Y.S. Soon, J. Electrochem. Soc. 148 (2001) A318.
[250] W.Y. Liu, Z.W. Fu, Q.Z. Qin, Thin Solid Films 515 (2007) 4045.
[251] H. Kitaura, K. Takahashi, F. Mizuno, A. Hayashi, K. Tadanaga, M. Tatsumisago, J. Electrochem. Soc. 154 (2007) A725.
[252] F. Kirino, Y. Ito, K. Miyauchi, T. Kudo, Nippon Kagaku Kaishi 3 (1986) 445.
[253] L. Jourdaine, J.L. Souquet, V. Delord, M. Ribes, Solid State Ionics 28 (1988) 1490.
[254] Y.Q. Chu, Q.Z. Qin, Chem. Mater. 14 (2002) 3152.
[255] F. Huang, Z.W. Fu, Y.Q. Chu, W.Y. Liu, Q.Z. Qin, Electrochem. Solid-state Lett. 7 (2004) A180.
[256] F. Huang, Z.W. Fu, Q.Z. Qin, Electrochem. Commun. 5 (2003) 262.
[257] J.F. Whitacre, W.C. West, E. Brandon, B.V. Ratnakumar, J. Electrochem. Soc. 148 (2001) A1078.
[258] M. Hayashi, M. Takahashi, Y. Sakurai, J. Power Sources 174 (2007) 990.
[259] N. Kuwata, N. Iwagami, Y. Tanji, Y. Matsuda, J. Kawamura, J. Electrochem. Soc. 157 (2010) A521.
[260] N. Kuwata, J. Kawamura, K. Toribami, T. Hattori, N. Sata, Electrochem. Commun. 6 (2004) 417.
[261] S. Jacke, J. Song, G. Cherkashinin, L. Dimesso, W. Jaegermann, Ionics 16 (2010) 769.
[262] B.J. Neudecker, R.A. Zuhr, J.D. Robertson, J.B. Bates, J. Electrochem. Soc. 145 (1998) 4160.
[263] H.K. Kim, T.Y. Seong, W.I. Cho, Y.S. Yoon, J. Power Sources 109 (2002) 178.
[264] R. Baskaran, N. Kuwata, O. Kamishima, J. Kawamura, S. Selvasekarapandian, Solid State Ionics 180 (2009) 636.
[265] J.J. Ding, Q. Sun, Z.W. Fu, Electrochem. Solid-state Lett. 13 (2010) A105.
[266] S.D. Jones, J.R. Akridge, F.K. Shokoohi, Solid State Ionics 69 (1994) 357.
[267] Y.S. Park, S.H. Lee, B.I. Lee, S.K. Joo, Electrochem. Solid-state Lett. 2 (1999) 58.
[268] N.J. Dudney, J.B. Bates, R.A. Zuhr, S. Young, J.D. Robertson, H.P. Jun, S.A. Hackney, J. Electrochem. Soc. 146 (1999) 2455.
[269] M. Baba, N. Kumagai, N. Fujita, K. Ohta, K. Nishidate, S. Komaba, H. Groult, D. Devilliers, B. Kaplan, J. Power Sources 97 (2001) 798.
[270] M. Baba, N. Kumagai, H. Fujita, K. Ohta, K. Nishidate, S. Komaba, B. Kaplan, H. Groult, D. Devilliers, J. Power Sources 119 (2003) 914.
[271] H. Nakazawa, K. Sano, M. Baba, J. Power Sources 146 (2005) 758.
[272] A. Eftekhari, J. Power Sources 132 (2004) 240.
[273] C.L. Li, Z.W. Fu, Electrochim. Acta 52 (2007) 6155.
[274] W.C. West, J.F. Whitacre, B.V. Ratnakumar, J. Electrochem. Soc. 150 (2003) A1660.
[275] C.L. Li, B. Zhang, Z.W. Fu, J. Electrochem. Soc. 153 (2006) E160.
[276] H. Nakazawa, K. Sano, T. Abe, M. Baba, N. Kumagai, J. Power Sources 174 (2007) 838.
[277] S.J. Lee, H.K. Baik, S.M. Lee, Electrochem. Commun. 5 (2003) 32.
[278] N. Kuwata, R. Kumar, K. Toribami, T. Suzuki, T. Hattori, J. Kawamura, Solid State Ionics 177 (2006) 2827.
[279] M. Baba, N. Kumagai, H. Kobayashi, O. Nakano, K. Nishidate, Electrochem. Solid-state Lett. 2 (1999) 320.
[280] S.H. Lee, P. Liu, C.E. Tracy, D.K. Benson, Electrochem. Solid-state Lett. 2 (1999) 425.
[281] J. Zhu, J.K. Feng, L. Lu, K.Y. Zeng, J. Power Sources 197 (2012) 224.
[282] W.C. West, J.F. Whitacre, J. Electrochem. Soc. 152 (2005) A966.